

Dilation of subglacial sediment governs incipient surge motion in glaciers with deformable beds

Brent M. Minchew¹ and Colin R. Meyer²

¹Department of Earth, Atmospheric and Planetary Sciences, Massachusetts Institute of Technology, Cambridge, MA, USA

²Thayer School of Engineering, Dartmouth College, Hanover, NH, USA

Abstract

Glacier surges are quasi-periodic episodes of rapid ice flow that arise from increases in slip-rate at the ice-bed interface. The mechanisms that trigger and sustain surges are not well-understood. Here, we develop a new model of incipient surge motion for glaciers underlain by sediments to explore how surges may arise from slip instabilities within this thin layer of saturated, deforming subglacial till. Our model represents the evolution of internal friction, porosity, and pore water pressure within the sediments as functions of the rate and history of shearing of the till. Changes in pore water pressure govern incipient surge motion, with less-permeable till facilitating surging because dilation-driven reductions in pore-water pressure slow the rate at which till tends toward a new steady state, thereby allowing time for the glacier to thin dynamically. The reduction of overburden pressure at the bed caused by dynamic thinning of the glacier sustains surge motion in our model. The need for changes in both the hydromechanical properties of the till and thickness of the glacier creates restrictive conditions for surge motion that are consistent with the rarity of surge-type glaciers and their geographic clustering.

Subjects: glaciology, geophysics, mathematical modeling

Keywords: glacier surges, glacier dynamics, granular mechanics

1 Introduction

Surges are enigmatic characteristics of glacier flow. Broadly speaking, glacier surges are sub-annual to multi-annual periods of relatively rapid flow that occur quasi-periodically, with quiescent periods between surges ranging from several years to centuries [1, 2]. Flow velocities during a surge can reach 5–100 times typical quiescent-phase velocities because of commensurate increases in the rate of slip at the ice-bed interface, hereafter called basal slip rate. Accelerated basal slip rates are facilitated by changes in the mechanical, thermal, and hydrological properties of the bed, which may work independently or in concert to initiate, sustain, and arrest glacier surges [2–10].

Surges are known to occur in only about 1% of glaciers worldwide [11, 12]. Known surge-type glaciers are clustered in a handful of globally dispersed geographic regions, share comparable geological factors, but inhabit a variety of climates [1, 12, 13]. A common feature identified in surge-type glaciers is the presence of mechanically weak beds consisting of thick layers of water-saturated, deformable sediment and erodible sedimentary or volcanic rock [14–17]. This commonality suggests that the mechanics of deformable glacier beds play an important role in initiating and sustaining glacier surges. However, the fact that not every glacier underlain by sediments surges indicates that the existence of a deformable bed is not a sufficient condition for surging [16]. Despite the prevalence of till, many existing surge models ignore till mechanics and consider only rigid, impermeable beds, often with a focus on the hydrological and thermal states [10, 18].

The prevailing model of glacier surges posits that incipient surge motion arises from a switch in the subglacial hydrological system from a relatively efficient channelized system to an inefficient distributed, or

38 linked-cavity, system [3, 10, 19]. Throughout the surge phase, the basal hydrological system likely remains
39 relatively inefficient, facilitating rapid basal slip due to lubrication from high basal water pressures, until
40 reestablishment of an efficient channelized system reduces basal water pressure and terminates the surge
41 [19–22]. Given a supply of water to the bed, this theory has the potential to explain rapid surge motion and
42 coincident increases in basal water pressure, at least in glaciers with rigid beds [19]. Indeed, observations of
43 a subglacial flood that occurred during, but did not initiate, a surge suggest that the basal hydrological system
44 was likely inefficient during the surge and became channelized just prior to surge termination [20, 23].
45 However, surges are often observed to begin in late fall or winter, when surface meltwater supplies are
46 limited [19, 21, 24–27]. As noted by Kamb [3], often credited with introducing hydrological switching as
47 an incipient surge mechanism, surge onset in the absence of surface meltwater flux may require an incipient
48 surge mechanism beyond a switch from an efficient to an inefficient basal hydrological system. Furthermore,
49 observations of numerous surge-type glaciers in Iceland show that jökulhaups, or subglacial floods, do not
50 cause surges despite massive, rapid increases in basal water flux that characterize jökulhaups [15], and
51 it remains unclear if hydrological models derived under the assumption of rigid, impermeable beds are
52 applicable to glaciers with till-covered beds. In any case, hydrological models have not explained the spatial
53 distribution of surge-type glaciers and it seems unlikely that such models can explain why most surge-type
54 glaciers reside on deformable beds. So while the connection between surging and subglacial hydrology may
55 be robust, the causal link between the efficiency of the basal hydrological system and surge motion remains
56 unclear.

57 Another model of glacier surges, first advocated by Robin [28], contends that sediment underlying a
58 polythermal glacier may freeze during the quiescent phase, strengthening the bed, similar to binge-purge
59 models for Heinrich events [29–31]. As ice collects in an upstream reservoir, the thickening ice increases
60 the overburden pressure at the bed, resulting in a corresponding decrease in the melting temperature of
61 ice that can cause the bed to thaw and, subsequently, weaken. Warm, weakened beds facilitate basal slip,
62 resulting in frictional heating that melts basal ice. Melted ice further lubricates the bed leading to enhanced
63 basal slip and more heating, thereby driving a positive thermal feedback loop [5, 32, 33]. Because thermal
64 control of glacier sliding requires ice to freeze to the bed, it cannot explain surging in temperate glaciers,
65 in which the ice is at the melting temperature and is unable to freeze to the bed. Recent observational
66 work shows that at least some surges in polythermal glaciers initiate in temperate zones, suggesting further
67 limitations on the applicability of thermal instability to incipient surge motion [34, 35] and indicating that
68 thermal instability is not a universal surge mechanism [32].

69 The prevalence of till layers beneath surge-type glaciers suggests that changes in the mechanical prop-
70 erties of till caused by dilation and variable pore water pressure are a promising complement to the previous
71 models of incipient surge mechanisms, which assume rigid, impermeable beds [10, 36]. It would be difficult
72 to overstate the complexity of granular mechanics in subglacial till [37], which is especially pronounced
73 where the till contains coarse clasts, where ice at the ice-bed interface is laden with debris [38–40], where
74 the ice slides over the ice-till interface [39, 41, 42], where clasts frozen into the ice can plow through the
75 till [43], and where the till is mobilized during surging [44]. Even within a relatively simple layer of near-
76 homogeneous sediment, we may expect multiple mechanisms to contribute to till deformation at any given
77 time, including grain boundary sliding, granular flow from comminution and grain rolling, and compaction
78 and dilation caused by shearing [45, 46]. Developing models that capture all of these mechanisms is an
79 active area of research, and we know of no current models that account for all mechanisms in a manner that
80 satisfyingly elucidates the underlying physics. Despite these challenges, notable surge models for glaciers
81 with deformable beds have been proposed by other authors. Truffer et al. [14, 47] inferred till mobilization
82 as a surge mechanism from direct observations of till deformation beneath a surge-type in Alaska. Wood-
83 ward et al. [17] proposed a conceptual model based on ice penetrating radar surveys of a surge-type glacier
84 in Svalbard that indicated imbricate thrust faulting. And Clarke [37] developed a physical framework for
85 subglacial till based in part on critical state soil mechanics and an assumed viscoplastic rheology for satu-

86 rated subglacial till.

87 Motivated in part by these models for surging in glaciers with deformable beds, we present a new physi-
88 cal model that leverages the mechanical properties of granular materials to help explain incipient surge mo-
89 tion in the absence of additional surface meltwater flux and frozen beds. Our model is informed by studies of
90 soil mechanics and earthquake nucleation and slow-slip events on tectonic faults containing water-saturated
91 gouge. Gouge and glacial till are mechanistically comparable materials in that both derive their strength
92 from a fine-grained matrix [37] and, in the cases of fault breccia and till, may feature coarse clasts [48].
93 Regardless of the presence of coarse clasts, the load is carried by the fine-grained matrix. Laboratory exper-
94 iments on fault gouge and till indicate that these materials have elastic-plastic rheologies with yield stresses
95 defined by the normal effective stress (the difference between overburden and pore fluid pressure) and the
96 tendency of the till to undergo internal frictional slip along grain boundaries [46, 49–57]. Shear strength is a
97 function of the rate of shearing within the till (hereafter called basal slip rate for glacier applications) and the
98 shear history of the till. Accounting for shear history is important because shearing can cause either dilation
99 or compaction of granular materials, depending on the state of consolidation in the material [58]. Dilation
100 has been identified through theory and observation as an important component controlling basal slip rates for
101 glaciers in Svalbard and Alaska, ice caps in Iceland, and ice streams in Antarctica [17, 47, 51, 54, 59–62],
102 and here we seek to better understand the role of till compaction and dilation in incipient surge motion by
103 developing a simple model that captures the relevant physical processes.

104 2 Model derivation

105 Consider a glacier with length ℓ , thickness h , and constant width $2w$, where $h \ll w \ll \ell$. Let us define a
106 coordinate system oriented such that x is along flow, y is across flow in a right-handed configuration, and z
107 is downward along the gravity vector (Fig. 1). Assume that ice thickness varies along-flow and is constant
108 across-flow such that $h = h(x)$.

109 Water-saturated till underlies the glacier. We divide the till into two layers separated by a *décollement*:
110 the top layer is deformable with thickness h_s and pore water pressure p_w , while the lower layer is a stationary,
111 non-deforming half-space with pore water pressure $p_{w\infty}$. Aside from strain rate, pore water pressure, and
112 otherwise stated properties, all physical properties of the till are assumed to be the same in both layers.
113 Our idealized glacier has a subglacial hydrological system that, like any glacier, evolves due to changes in
114 meltwater flux and basal slip rate [63–65]. Here we assume that both the state of the hydrological system and
115 the basal water flux are accounted for in p_{w_r} , the water pressure within the hydrological system, depicted as
116 a reservoir in the system diagram (Fig. 1).

117 We assume that basal slip is due entirely to deformation of the upper till layer, meaning that p_{w_r} only
118 influences ice flow through its influence on p_w . We make this simplifying assumption in spite of the fact that
119 p_{w_r} may cause sliding of the ice relative to the bed [64, 66–69] because our focus is on how the mechanical
120 properties of till might induce surging in the absence of externally sourced meltwater flux. Unless there is a
121 significant flux of meltwater into the subglacial hydrological system, an unlikely scenario during winter, p_{w_r}
122 should remain approximately constant in time when averaged over a spatial scale of order the ice thickness.
123 This assumption of nearly constant wintertime p_{w_r} is merely conceptual and is not a necessary condition in
124 the subsequent derivation because time-varying p_{w_r} is accounted for in the model. Indeed, in future work,
125 subglacial hydrological models could be readily bolted onto the model presented here. For simplicity, we
126 ignore potential changes in pore water pressure caused by plowing particles [39, 43], and begin our study at
127 the glacier bed with an exploration of till mechanics.

128 2.1 Mechanical properties of till

129 We adopt a phenomenological model for the mechanical strength of till that depends on basal slip rate u_b
 130 and the state of the subglacial till θ . This rate-and-state friction model accounts for instantaneous basal slip
 131 rate and, importantly, basal slip history, and was derived to explain numerous laboratory measurements of
 132 sliding on bare rock and granular interfaces. Rate-and-state friction is widely used in studies of earthquake
 133 nucleation and slow-slip events on tectonic faults, and gives the instantaneous shear strength of subglacial
 134 till as [49, 50]

$$\tau_t = N\mu = N \left[\mu_n + a \ln \left(\frac{u_b}{u_{b_n}} \right) + b \ln \left(\frac{\theta u_{b_n}}{d_c} \right) \right], \quad (1)$$

135 where μ_n is the coefficient of nominal internal friction, d_c is a characteristic slip displacement, u_{b_n} is a
 136 constant reference velocity, and the constants a and b are material parameters that define the magnitude of
 137 the direct (velocity) and evolution (state) effects, respectively. As we will discuss, b is important for this
 138 study at it encodes the effect of dilation on the bulk friction coefficient μ . In our idealized glacier geometry,
 139 the bed is horizontal and effective normal stress is equal to effective pressure, defined as

$$N = p_i - p_w, \quad (2)$$

$$p_i = \rho_i g h, \quad (3)$$

140 where ρ_i is the mass density of ice, g is gravitational acceleration, p_i is the ice overburden pressure, and p_w
 141 is the pore water pressure within the till.

142 Rate-and-state friction has received attention in studies of the ice-bed interface [36, 39, 42, 70, 71] and
 143 is widely studied for slip on tectonic faults containing gouge [72–75], a material mechanistically similar to
 144 till [76]. Though distinct in many respects, earthquakes and glacier surges are analogous in the sense that
 145 both involve long quiescent periods and relatively short activation timescales. Slow-slip on tectonic faults
 146 are particularly relevant to studying glacier surges because of their comparable slip durations and slow slip
 147 rates compared with major earthquakes [74, 77]. Incipient motion in both earthquakes and glacier surges is
 148 brought on by excess applied stress relative to frictional resistance. While stresses and displacement rates
 149 are orders of magnitude higher in earthquakes than in glaciers, the experimentally verified rate-and-state
 150 friction model is applicable to glacier surges as there is no known lower bound on velocity for the model to
 151 be valid [78].

152 When till is deformed, individual grains are mobilized by cataclastic flow (which includes grain rolling
 153 and boundary sliding), dilation, and comminution. Under small displacements, the granular structure of the
 154 till is related to the pre-deformed structure, meaning that the till essentially remembers its prior state. Mem-
 155 ory is represented by the state variable θ , and is lost as the glacier slips over a characteristic displacement
 156 d_c . Steady state till shear strength occurs when state evolution ceases ($\dot{\theta} = 0$) and is defined as

$$\hat{\tau}_t = N \left[\mu_n + (a - b) \ln \left(\frac{\hat{u}_b}{u_{b_n}} \right) \right], \quad (4)$$

157 where $\hat{u}_b = d_c / \hat{\theta}$ is the steady state basal slip rate. (Hereafter, hatted values indicate steady state for the
 158 respective variable.) As we shall soon see, d_c is the slip distance over which state (and porosity) evolve, but
 159 it has also been interpreted as the slip distance at which the (rate-weakening) stress reduces to the residual
 160 stress [79]. Computational and microphysical studies have concluded that d_c is proportional to the thickness
 161 of the deforming layer [75, 80, 81], which can be expected to be of order 0.1–1 m in subglacial till and varies
 162 with permeability [53, 82]. Other factors influencing d_c include grain size and porosity [75].

163 State, θ , has dimensions of time. It has been taken to represent the product of the contact area and
 164 intrinsic strength (quality) of the contact [83], but also has been interpreted as the average age of contacts
 165 between load-bearing asperities [84]. Under either interpretation, state is expected to evolve as a function

166 of time, slip, and effective normal stress [49, 84–86]. To represent the evolution of θ , we adopt what is
 167 commonly referred to as the slip law [50]

$$\dot{\theta} = -\frac{\theta u_b}{d_c} \ln \left(\frac{\theta u_b}{d_c} \right), \quad (5)$$

168 which dictates that state evolves only in the presence of slip. The only stable steady state in Eq. 5 exists at
 169 $\theta = d_c/u_b$; when $u_b > 0$, θ always tends toward the stable steady state. Increasing u_b beyond d_c/θ , through
 170 enhanced surface meltwater flux, calving, or other external forcing, will reduce θ over time. Similarly, when
 171 $u_b < d_c/\theta$, θ will increase toward steady state. In the next section we show that changes in θ are brought
 172 about through till compaction and dilation. As such, θ accounts for the basal slip history and plays a key
 173 role in determining bed strength and the response of bed strength to shear and external forcing.

174 2.2 Pore water pressure

175 Till shear strength is proportional to effective pressure (Eq. 1), the difference between overburden and pore
 176 water pressure (Eq. 2). Assuming that the mass density of ice remains constant, effective pressure can only
 177 vary during surges due to changes in ice thickness and pore water pressure. Pore water pressure is linked to
 178 till compaction and dilation through changes in the effective till porosity. Thus, if we assume that the till is
 179 always saturated, then the rate of change of water mass per unit volume within the till is given as

$$\dot{m}_w = \rho_w \dot{\phi}, \quad (6)$$

180 where ϕ is the (dimensionless) effective till porosity, defined as the ratio of pore volume to total volume, and
 181 ρ_w is the density of water. In this section, we seek to understand the rate of change in pore water pressure
 182 as a function of basal slip rate under the basic assumptions that water is incompressible over the range of
 183 reasonable subglacial pressures and that frictional heating at the ice-bed interface and plastic dissipation
 184 within the till are negligible.

185 2.2.1 Evolution of porosity

186 Assuming that individual grains in the till are rigid, strain within the till will be accommodated by changes
 187 in porosity. Adopting an elastic-plastic model for the deformation of granular till, wherein the total strain
 188 is equal to sum of the elastic and plastic strains, we separate porosity changes into a plastic component, $\dot{\phi}_p$,
 189 and an elastic component $\dot{p}_w \beta$ such that [73, 87]

$$\dot{\phi} = \dot{p}_w \beta + \dot{\phi}_p, \quad (7)$$

where

$$\beta = \frac{\partial \phi}{\partial p_w} = \frac{\epsilon_e (1 - \phi)^2}{N} \quad (8a,b)$$

190 is the till compressibility and ϵ_e is the elastic compressibility coefficient, taken to be in the range $\epsilon_e \sim 10^{-3}$ –
 191 10^{-1} [88]. Following work by Segall and Rice [73] and Segall et al. [77] on slow-slip events on tectonic
 192 faults, we take the plastic component of porosity to have the same form as the evolution component of the
 193 rate-and-state model for till shear strength (Eq. 1), namely

$$\dot{\phi}_p = \dot{\phi}_c - \epsilon_p \ln \left(\frac{\theta u_{bn}}{d_c} \right), \quad (9)$$

194 where ϕ_c is a (constant) characteristic porosity and ϵ_p is a dilatancy coefficient, a dimensionless parameter
 195 hereafter assumed constant and in the range $10^{-4} \leq \epsilon_p \leq 10^{-2}$ [77]. We note that the only sensitivity
 196 in our model to the absolute value of ϵ_p is to the evolution of porosity; surge behavior, the main focus of
 197 this study, is influenced only by the ratio ϵ_p/β , which represents the relative importance of each term in
 198 Eq. 7. By adopting Eq. 9, we are assuming that plastic deformation of the till is completely determined by
 199 changes in state, θ , the only variable in Eq. 9. This assumption is physically justifiable: irreversible changes
 200 in porosity necessitate a change in the average age of granular contacts and, equivalently, a change in the
 201 product of the contact area and quality, both of which are the physical interpretations of state discussed
 202 above. Differentiating Eq. 9 in time yields

$$\dot{\phi}_p = -\epsilon_p \frac{\dot{\theta}}{\theta}, \quad (10)$$

203 an expression that indicates that shearing causes till to compact ($\dot{\phi}_p < 0$) when θ is below steady state
 204 ($\theta < d_c/u_b$) and to dilate when θ is above steady state. Such behavior is consistent with observations of
 205 the response of over- and under-consolidated soils to shear [58]. As we will show, the relationship between
 206 plastic till deformation and state will give rise to rich mechanical relationships between compaction, dilation,
 207 and shearing, as is expected from sediments.

208 2.2.2 Evolution of pore water pressure

209 Let us now consider water flux in the till in response to changes in porosity and sources outside the till shear
 210 layer. The rate of change of water mass is given by plugging the expressions for the total rate of change in
 211 porosity (Eq. 7) and the rate of irreversible (plastic) change in porosity (Eq. 10) into the expression for the
 212 rate of change in mass per unit volume (Eq. 6) yielding

$$\dot{m}_w = \rho_w \dot{p}_w \beta + \rho_w \epsilon_p \frac{u_b}{d_c} \ln \left(\frac{\theta u_b}{d_c} \right). \quad (11)$$

213 Conservation of water mass gives

$$\frac{\partial q_w}{\partial z} + \dot{m}_w = 0, \quad (12)$$

214 where q_w is the water mass flux and we have assumed horizontal gradients in water pressure are negligible
 215 compared with vertical gradients. Taking the basal ice to be impermeable requires water flux to be entirely
 216 into and out of the bed. Under these conditions, Darcy's law is given as

$$q_w = -\frac{\rho_w \gamma_h}{\eta_w} \frac{\partial p_w}{\partial z}, \quad (13)$$

217 where γ_h is the till permeability and η_w is the dynamic viscosity of water. Combining Eqs. 11–13 under the
 218 assumption that till permeability is spatially constant and independent of porosity gives

$$\dot{p}_w = \kappa_h \frac{\partial^2 p_w}{\partial z^2} + \frac{\epsilon_p \dot{\theta}}{\epsilon_e \theta} \frac{N}{(1 - \phi)^2}, \quad (14)$$

219 where

$$\kappa_h = \frac{\gamma_h}{\eta_w \beta}, \quad (15)$$

220 is the hydraulic diffusivity of the deforming till layer. Measurements of hydraulic diffusivity in till give a
 221 range for κ_h of approximately 10^{-9} – 10^{-4} m²/s, with a strong sensitivity to clay content [89, 90]. We take
 222 constant effective permeability to be a reasonable first approximation given the small change in permeability
 223 under glaciologically relevant pressures and strains found in discrete element modeling studies [82]. A more

224 general treatment of pore water pressure evolution would include a porosity-dependent permeability in place
 225 of a constant effective permeability — for example, the Kozeny-Carman model used by [37]. We reserve
 226 this additional complexity for future work as our simple model retains the salient physical processes.

227 Shearing in till concentrates in a thin, multi-layer zone that is typically several centimeters thick [54, 91–
 228 93]. We therefore approximate

$$\frac{\partial^2 p_w}{\partial z^2} = \frac{p_{w_\infty} - 2p_w + p_{w_r}}{h_s^2}, \quad (16)$$

229 where h_s is the thickness of the shear zone in the till, p_{w_∞} is the water pressure in the underlying permeable
 230 half space, and p_{w_r} is the water pressure in the basal hydrological system (Fig. 1). With this approximation,
 231 Eq. 14 becomes

$$\dot{p}_w = \frac{p_{w_\infty} - 2p_w + p_{w_r}}{t_h} + \frac{\epsilon_p \dot{\theta}}{\epsilon_e \theta} \frac{N}{(1 - \phi)^2}, \quad (17)$$

232 where the first term represents Darcian flow into and out of the deforming till layer and the second term
 233 represents dynamical (dilation-driven) changes in pore water pressure. The Darcy-flow component of pore
 234 water pressure evolution is inversely proportional to the characteristic diffusive timescale for pore water in
 235 the deforming till layer

$$t_h = \frac{h_s^2}{\kappa_h}. \quad (18)$$

236 To simplify the analysis, we hereafter take t_h to be constant, thereby ignoring the dependence of κ_h and
 237 h_s on effective pressure N and porosity ϕ . We justify this simplification by noting that κ_h (Eq. 15) and
 238 till thickness h_s roughly scale as N , though a detailed analysis of the relation between h_s and N is beyond
 239 the scope of this work [37]. Assuming $h_s \sim N$ and $\kappa_h \sim N$, $t_h \sim N$ to a reasonable approximation and
 240 therefore should retain the same order of magnitude during incipient surge motion. Similarly for permeabil-
 241 ity, where compaction-driven reductions in permeability will induce relatively small (factor of 2) decreases
 242 in thickness h_s [82]. Such small changes are unlikely to dramatically alter the dynamics of surge motion
 243 captured here, and we leave for future work a more detailed analysis involving variable t_h .

244 From the second term in Eq. 17, we can see that the sign of the dynamical (or dilation-driven) component
 245 of \dot{p}_w is determined by the state of the till relative to steady state. When state, θ , is below (above) steady
 246 state and $t_h > 0$, pore water pressure will increase (decrease) until steady state is achieved. These changes
 247 in pore water pressure are entirely due to changes in till porosity: compaction ($\dot{\phi}_p < 0$) results in faster rates
 248 of change in the dynamical component of water pressure because $\epsilon_p \dot{\theta} N / [\epsilon_e \theta (1 - \phi)^2] = -\dot{\phi}_p / \beta$. Whether
 249 p_w increases or decreases following step changes in basal slip rate depends on the whether the ratio $\theta u_b / d_c$
 250 is greater than or less than unity.

251 2.3 Basal slip acceleration

252 Glacier ice is an incompressible viscous fluid in laminar flow, and the momentum equation, incompressibil-
 253 ity condition, and continuity equation, respectively, take the forms

$$0 = \frac{\partial \tau_{ij}}{\partial x_j} - \frac{\partial \tilde{p}}{\partial x_i} + \rho_i g \delta_{iz}, \quad (19)$$

$$0 = \frac{\partial u_i}{\partial x_i}, \quad (20)$$

$$\dot{h} = \dot{M} - \frac{\partial}{\partial x_i} (h \bar{u}_i), \quad (21)$$

254 where u_i is the ice velocity vector, \bar{u}_i is the depth-averaged ice velocity vector, τ_{ij} is the deviatoric stress
 255 tensor, δ_{ij} is the Kronecker delta, \tilde{p} is the mean isotropic ice stress (pressure), \dot{M} is the total surface mass

256 balance (which includes surface and basal mass balance and is positive for mass accumulation), and we em-
 257 ploy the summation convention for repeated indices. To simplify our analysis, we neglect vertical shearing
 258 in the ice column, and adopt a depth-integrated momentum equation (often referred to as the shallow shelf
 259 approximation) [94]

$$2 \frac{\partial}{\partial x} (h\tau_{xx}) + \frac{\partial}{\partial y} (h\tau_{xy}) + \tau_b = \tau_d, \quad (22)$$

260 where τ_{xx} is the extensional deviatoric stress, τ_{xy} the lateral shear stress, and we have neglected the trans-
 261 verse normal (deviatoric) stress τ_{yy} . In some surge-type glaciers, vertical shearing may be the dominant flow
 262 regime during the quiescent phase, while basal slip is the dominant flow regime during the surge phase. Eq.
 263 22 is valid only when basal slip is dominant, and thus a model of basal slip acceleration derived from Eq.
 264 22 may not fully detail glacier flow during incipient surge acceleration in some glaciers. Nevertheless, this
 265 simplification is reasonable because the focus of this work is on till mechanics and the flow model based on
 266 Eq. 22 will represent the salient processes of nascent surge acceleration. We reserve for future work a more
 267 detailed analysis that retains more components of the stress divergence and is able to capture the transition
 268 from vertical-shear-dominated flow to basal-slip-dominated flow.

269 Force balance dictates that basal shear traction cannot exceed the lesser of applied stress and yield stress
 270 of the till, giving rise to the relation [44, 95]

$$\tau_b = \min(\tau_d, \tau_t), \quad (23)$$

271 where $\tau_t = \mu N$ is the till shear strength (Eq. 1) and the gravitational driving stress is defined as

$$\tau_d = \rho_i g h \alpha \quad (24)$$

272 where α is the ice surface slope, assumed small such that $\sin(\alpha) \approx \alpha$. Recall that we are focusing on the
 273 case in which rapid flow during the surge is accommodated primarily by deformation of the bed, giving rise
 274 to the relations $\tau_b = \tau_t$ and $u_s \approx u_b$.

275 Let us now focus only on the region where the surge is initiated and assume the areal extent of incipient
 276 surge motion is large enough to make the gradient of longitudinal stress (first term in Eq. 22) negligible
 277 during the nascent surge phase. Taking ice to be shear-thinning fluid, the constitutive relation, commonly
 278 known as Glen's law [96], is

$$\dot{\epsilon}_e = A \tau_e^n, \quad (25)$$

279 where $\dot{\epsilon}_e = \sqrt{\dot{\epsilon}_{ij}\dot{\epsilon}_{ij}/2}$ is the effective strain rate, $\tau_e = \sqrt{\tau_{ij}\tau_{ij}/2}$ is the effective deviatoric stress, the rate
 280 factor A is a scalar, and the stress exponent is $n = 3$. Hereafter, A and n are assumed constant. Under
 281 our prior assumptions, $2\dot{\epsilon}_e \approx \partial u_b / \partial y$ and $\tau_e \approx \tau_{xy}$. Integrating the reduced form of Eq. 22 twice along y
 282 subject to the symmetry condition $\tau_{xy} = 0$ at the centerline and no-slip condition at the margins gives the
 283 centerline basal slip rate

$$u_b = u_r \left[\alpha - \mu \left(1 - \frac{p_w}{p_i} \right) \right]^n, \quad (26)$$

284 where

$$u_r = \frac{2A(\rho_i g)^n}{n+1} w^{n+1}, \quad (27)$$

285 is a reference velocity. Taking u_r and w to be constants and differentiating Eq. 26 with respect to time yields
 286 an expression for acceleration in basal slip

$$\dot{u}_b = nu_b \left[\frac{\dot{\alpha} - \mu \frac{p_w}{p_i} \left(\frac{\dot{h}}{h} - \frac{\dot{p}_w}{p_w} \right) - b \frac{\dot{\theta}}{\theta} \left(1 - \frac{p_w}{p_i} \right)}{\alpha + (an - \mu) \left(1 - \frac{p_w}{p_i} \right)} \right], \quad (28)$$

287 where the rates of change in glacier geometry (\dot{h} and $\dot{\alpha}$), pore water pressure (\dot{p}_w), and state ($\dot{\theta}$) all contribute
 288 to the basal slip acceleration, along with instantaneous geometry (h and α), pore water pressure (p_w), state
 289 (θ), and basal slip rate (u_b). Note that the conditions $\tau_d > \tau_b$ and $\tau_b = \tau_t$, discussed and imposed earlier in
 290 this section, ensure that the denominator in Eq. 28 is always greater than zero.

291 Eq. 28 is the central result of this study. This formula describes the dependence of surge acceleration
 292 on glacier geometry, pore water pressure, and the properties of the till. The terms in the numerator can be
 293 related to the processes of interest during the surge. Namely, the first term in the numerator ($\dot{\alpha}$) essentially
 294 represents the rate of change in the gravitational driving stress. The second term in the numerator captures
 295 the evolution of effective pressure (N), which governs the shear strength of the bed. The third and final
 296 term in the numerator accounts for the influence of dilation on the internal friction coefficient of the till. We
 297 spend the remainder of this study investigating the influence of the various physical processes represented
 298 in Eq. 28.

299 **3 Results**

300 Since shear strength of the till is the governing factor in surge motion and is defined by three variables
 301 (overburden pressure p_i , pore water pressure p_w , and the internal friction coefficient μ), we present the
 302 results in three sections. In the first section, we discuss the evolution of pore water pressure following an
 303 increase in basal slip rate. Second, we consider the acceleration of basal slip for a glacier with a fixed
 304 geometry (*i.e.*, fixed overburden pressure). Lastly, we explore the full model, which allows for variations in
 305 pore water pressure, glacier geometry, and internal friction coefficient for till.

306 **3.1 Evolution of pore water pressure**

307 Pore water pressure in the deforming till layer evolves due to dilation and compaction of the till as well as
 308 through the exchange of water between the deforming till layer, the subglacial hydrological system, and the
 309 stagnant till layer that underlies the deforming layer (Eq. 17 and Fig. 2). In our model, the pressures in the
 310 stagnant till layer and the subglacial hydrological system are assumed constant in time, and the flow of water
 311 into or out of the deforming till layer is described by Darcy’s law (Eq. 13). Using the parameter values given
 312 in the caption of Fig. 2, we integrate Eqs. 5, 7, and 17 forward in time from the initial conditions $u_{b0} = 10$
 313 m/yr, $\phi_0 = 0.1$, $\theta_0 = d_c/u_{b0}$, and $p_{w0} = p_{w_r} = p_{w_\infty}$ using the variable-coefficient ordinary differential
 314 equation (VODE) solver implemented in SciPy (version 1.3.1), an open-source Python toolkit [97].

315 The results shown in Fig. 2 illustrate how the evolution of pore water pressure p_w following a step
 316 increase in basal slip rate is influenced by the hydraulic diffusion timescale of the deforming till layer (t_h)
 317 and the relative values of the elastic (ϵ_e) and plastic (ϵ_p) compressibility coefficients. Note that because we
 318 hold t_h fixed in time, only the relative compressibility ratio ϵ_e/ϵ_p influences pore water pressure, not the
 319 absolute values of ϵ_e and ϵ_p . All cases shown in Fig. 2 start at steady state and indicate initial decreases in
 320 pore water pressure p_w in response to till dilation followed by a return to steady state ($p_{w0} = p_{w_r} = p_{w_\infty}$)
 321 via Darcian flow over a timescale proportional to the diffusion timescale. The minimum pore water pressure
 322 is determined by the diffusion timescale t_h and the relative compressibility ϵ_e/ϵ_p . For a given relative
 323 compressibility, longer diffusion timescales, corresponding to lower till permeabilities, lead to a greater
 324 drop in pore water pressure (Fig. 2, upper panel). For a given diffusion timescale, smaller values of relative
 325 compressibility, which indicate stronger dilatancy of the till relative to poroelastic effects, result in greater
 326 drops in pore water pressure (Fig. 2, lower panel).

3.2 Acceleration with fixed ice thickness

We now consider glacier acceleration. As a first step, we simplify our analysis by assuming that the timescale of interest is longer than the timescale for pore water diffusion ($t > t_h$) but short enough to allow us to reasonably neglect changes in glacier geometry. While it can be argued that this condition may be physically contrived in some cases, it is useful for exploring surge dynamics and the behavior of the till in the absence of some complicating factors (in the next section we will allow glacier geometry to evolve). After fixing glacier geometry by imposing $\dot{h} = 0$ and $\dot{\alpha} = 0$ at all times, we solve the system of equations defined by Eqs. 5, 7, 17, and 28. For all results discussed here, we prescribe as the initial velocity $u_b = 1.1\hat{u}_b$ at $t = 0$, where $\hat{u}_b = 10$ m/yr, and set the initial values for all other variables to their respective steady state values. The system of equations is stiff, and therefore, we integrate forward in time using an implicit Runge-Kutta method — specifically the Radau IIA fifth-order method — implemented in SciPy (version 1.3.1).

In the cases shown in Fig. 3, we focus on the influences of a range of viable evolution effects (b values; indicated by line intensity and thickness) and different hydraulic diffusion timescales (t_h ; indicated by colors). Aside from b and t_h , all parameters are the same for all cases and are listed in the Fig. 3 caption. Note that $a = 0.013$, so in terms of the till friction coefficient μ , the cases shown in Fig. 3 are both rate-weakening ($a < b$; solid lines) and rate-strengthening ($a > b$; dashed lines).

The most notable feature in all cases shown in Fig. 3 is the lack of unstable acceleration. Steady state speed is governed by the steady state shear strength of till (Eq. 4) and is therefore sensitive to the rate-and-state parameters ($a - b$) and μ_n . Since the direct effect (a) is constant all cases in Fig. 3, increasing the evolution effect (b) leads to a greater steady state stress drop and faster steady state basal slip rate due to the increasingly negative value ($a - b$). The steady state values for all state variables are independent of the diffusion timescale t_h and characteristic slip length d_c . The primary influences of t_h and d_c are on the time the system take to reach steady state and the peak change in pore water pressure. These results show that the system tends to steady state over a characteristic timescale that scales with the (dimensionless) hydraulic transmittance

$$\psi_0 = \frac{\epsilon_p \hat{u}_{b0} t_h}{\epsilon_e d_c} \quad (29)$$

defined as the ratio of the hydraulic diffusion timescale t_h to the timescale for dilation-driven changes in pore water pressure $d_c \epsilon_e / (\epsilon_p u_{b0})$. The dependence on ψ_0 of the time to steady state is indicated in Fig. 3 by noting that the only term in ψ_0 that changes between the difference cases is the hydraulic diffusivity κ_h (and, consequently, t_h). The time axes in Fig. 3 are normalized by $d_c \epsilon_e / (\epsilon_p u_{b0})$, the timescale for dilation-driven changes in pore water pressure to help show that model realizations in which the diffusion timescale t_h is an order of magnitude longer, take an order of magnitude longer time to evolve to steady state. As we show in the next section, the time required to reach steady state is a crucial factor governing whether or not a glacier surges.

The behavior of the model in the absence of changes in glacier geometry (Fig. 3) provides further insight that help explain some of the results of the full model presented in the next section. For instance, the till dilates in all cases due to initial step and subsequent changes in basal slip rate (Fig. 3). The amplitude of the change in till porosity scales with the evolution parameter b , with larger values of b resulting in greater dilatancy. As seen in the previous section, higher dilatancy results in a larger drop in pore water pressure as the glacier accelerates. Dilatancy also drives a reduction in the internal friction coefficient of till, as a dilated till provides less resistance to shearing due to reduced contact areas between grains. This drop in the internal friction coefficient commensurately reduces the shear strength of the till.

3.3 Acceleration with variable ice thickness

Over longer timescales, dynamically driven changes in glacier geometry can be important, and we must consider the full expression given in Eq. 28. To do so, we approximate changes glacier geometry by

371 recalling that h varies only in the along-flow (x) direction and focusing only on the central trunk of the
 372 glacier where across-flow variations in the depth averaged velocity vector \bar{u} can be neglected. Thus, the
 373 continuity equation (Eq. 21) becomes

$$\dot{h} = \dot{M} - \frac{\partial}{\partial x} (\zeta h u_s), \quad (30)$$

374 where $\zeta = \bar{u}/u_s$, \bar{u} is the depth-averaged glacier speed, and u_s is the glacier surface speed. Since we have
 375 taken ice to be a non-Newtonian viscous fluid, we have $(n + 1)/(n + 2) \leq \zeta \leq 1$, where n is the stress
 376 exponent in the constitutive relation for ice (Eq. 25). In this study, we adopt the most common value for
 377 the stress exponent, $n = 3$, and we prescribe $\zeta = 1$ for consistency with the reduced momentum equation
 378 in Eq. 22 (when $\zeta = 1$, $u_s = u_b$). We further simplify the expression for dynamical thinning by neglecting
 379 extensional strain rates (consistent with the assumptions in §22.3), yielding

$$\dot{h} = \alpha \zeta (u_* - u_b), \quad (31)$$

where $u_* = \dot{M}/(\alpha \zeta)$ is the balance velocity. Finally, the rate of change in surface slope becomes

$$\dot{\alpha} = -\frac{\partial \dot{h}}{\partial x} \approx \frac{\dot{h} \alpha}{h} \quad (32a,b)$$

380 where Eq. 32b follows from the assumption of a parabolic surface profile for the glacier [88]. These
 381 approximations complete the quasi-1D model, and we solve Eqs. 5, 17, 28, 31, and 32 using the numerical
 382 solver described in §33.2.

383 The results, shown in Fig. 4, indicate markedly different behavior from the case where glacier geometry
 384 was held fixed (§33.2). Most notably, surging — defined here as an order of magnitude increase in basal slip
 385 rate — occurs for some combinations of the evolution parameter b and diffusion timescale t_h . In particular,
 386 for our chosen parameters (given in the Fig. 4 caption), higher b values and longer t_h times result in surges.
 387 On the other hand, b values and t_h times too small and/or short to generate surge behaviors produce prosaic
 388 glacier dynamics (small b , short t_h) or abandoned surges (small b , long t_h), the latter of which we define
 389 as a period of rapid flow speeds (factor of two or more faster than quiescent speeds) that do not meet the
 390 definition of a surge, followed by a slowdown and evolution to steady state. To clarify the distinction: Initial
 391 acceleration is unstable in surges and stable in abandoned surges.

392 To explore the processes that govern whether a surge develops, is abandoned, or is essentially absent,
 393 let us focus on some illustrative cases shown in Fig. 4. We start with two prominent cases: those with
 394 the highest b values (and therefore the heaviest lines in Fig. 4) and different hydraulic diffusivities (*i.e.*, t_h
 395 values). The case with $b = 0.05$ and higher diffusivity (and, consequently, higher hydraulic permeability
 396 and shorter t_h), shown with the heavy red lines in Fig. 4, undergoes an abandoned surge, defined by a
 397 brief acceleration phase, resulting in a maximum velocity of approximately twice the steady state slip rate
 398 ($u_b/\hat{u}_{b_0} \approx 2$), followed by deceleration and evolution to steady state. In this case, the glacier thins some-
 399 what, but the till tends to steady state before there is any marked change in the effective pressure at bed (N).
 400 The case with $b = 0.05$ and lower hydraulic diffusivity (heavy blue line) surges, with muted acceleration
 401 (relative to the case with higher hydraulic diffusivity) preceding a continual reduction in state, pore water
 402 pressure, ice thickness, and till internal friction coefficient. The rates of change in each of these values when
 403 the integration was terminated (at $u_b/\hat{u}_{b_0} = 10$) show that the glacier would continue to accelerate in the
 404 absence of contravening processes, such as increases in extensional stresses, that are not considered in our
 405 model but could manifest in a natural glacier. It is important to note that the effective pressure N continually
 406 decreases despite reductions in pore water pressure p_w because of the dynamic thinning of the glacier. In
 407 other words, reductions in overburden pressure $p_i = \rho_i g h$ outpace reductions in pore water pressure p_w ,
 408 leading to a net decrease in $N = p_i - p_w$ that complements reductions in the friction coefficient μ , ensuring

409 that basal drag ($\tau_b = \tau_t = N\mu$) diminishes in time. Sustained acceleration of the glacier unequivocally
410 indicates that the decline of basal drag outpaces thinning-induced reductions in gravitational driving stress.

411 Other cases shown in Fig. 4 indicate the same basic behavior: till with higher values of hydraulic
412 permeability allows for faster acceleration, which causes the till to evolve to steady state before significant
413 thinning of the glacier can occur. Rates of acceleration and evolution to steady state are slower in less-
414 permeable till, allowing rapid ice flow to persist for longer periods of time, facilitating dynamic thinning of
415 the glacier. Longer timescales with relatively muted acceleration allow for thinning because dynamic glacier
416 thinning scales as the time-integral of ice velocity (Eq. 31), meaning that longer periods of moderately rapid
417 flow can produce more thinning than much short periods of somewhat faster flow. These results suggest that
418 it is the reduction in overburden pressure p_i , and therefore effective pressure N , through dynamic thinning
419 that is ultimately responsible for sustaining surge motion. The lack of unstable acceleration when glacier
420 geometry is fixed in time (discussed in the previous section) and the manifestation of surging in cases of rate-
421 strengthening friction coefficients (dashed lines in Fig. 4) both serve to highlight importance of dynamic
422 thinning for sustaining surge motion.

423 The evolution of till porosity, as shown in Fig. 4, is markedly different from the case with fixed glacier
424 geometry (previous section). Till consistently dilated when glacier geometry was fixed because effective
425 pressure decreased then returned to steady state along with water pressure. But the dependence of the rate
426 of change in till porosity on the effective pressure via β (Eqs. 7 and 8) results in net compression when we
427 allow the glacier to thin. As effective pressure decreases due to thinning of the glacier, the sensitivity of
428 the rate of change in porosity due to changes in pore water pressure become more pronounced. Since pore
429 water pressure decreases in response to the evolution of till state (Eq. 17), the net effect is till compaction
430 that lags reductions in pore water pressure.

431 The results discussed in this section indicate that the principal factors governing the surge behavior of a
432 glacier are the hydraulic diffusion timescale of the deforming till layer, t_h , the relative compressibility ϵ_e/ϵ_p ,
433 and the evolution parameter b , the latter of which dictates the response of the internal friction coefficient
434 to till dilation. We explore this parameter space in Fig. 5; except where indicated, model parameters
435 are the same as for Fig. 4, and we use the same numerical solver. The results in Fig. 5 show that for
436 any relative compressibility ϵ_e/ϵ_p , surge-type behavior is favored in glaciers with high b values and long
437 diffusion timescales (*i.e.*, relatively impermeable beds). Higher b values imply a greater reduction in the
438 internal friction coefficient of till (μ) in response to changes in porosity (and therefore, state), with rate-
439 weakening values ($b > a$) resulting in a reduced steady state friction coefficient. Positive glacier acceleration
440 is generally expected as the friction coefficient decreases in response to state evolution, causing surges to
441 be favored at higher b values. As previously discussed, longer diffusion timescales (*i.e.*, lower hydraulic
442 permeability) diminish the rate of porosity (state) evolution, and therefore, slows dilatant hardening effects.
443 Thus, slow diffusion of pore water enables a longer acceleration period that allows time for dynamic glacier
444 thinning to drive a net reduction in the effective pressure. Surge-type glaciers are more likely to manifest
445 in tills that have a high relative compressibility, $\epsilon_e/\epsilon_p > 10$, as these higher values imply less dilatant
446 hardening (the reduction in pore water pressure due to shearing; cf. Fig. 2).

447 The rich dynamical behavior illuminated in Fig. 5 is enhanced by the manifestation of regions (in the
448 parameter space) of abandoned surges adjacent to the regions of surging behavior. Abandoned surge regions
449 are indicated in Fig. 5 by maximum basal slip rates greater than the initial value ($u_{b_{max}}/\hat{u}_{b_0} > 2$, as shown
450 in purple-to-red hues) and final basal slip rates less than the initial value ($u_{b_{final}}/\hat{u}_{b_0} < 0.5$, as shown in
451 grey tones). Abandoned surges manifest only where b values are relatively large but not large enough to
452 produce a surge and diffusion timescales are slightly too short to allow for a full surge. According to our
453 results, it is possible for a glacier to exhibit abandoned surges for any value of ϵ_e/ϵ_p , but the region in the
454 parameter space that produces abandoned surges increases with ϵ_e/ϵ_p (*i.e.*, as dilatant hardening decreases).

455 Two other remarkable and persistent features of the parameter space are worth highlighting. First, aban-
456 doned surge regions are accompanied by an area of the parameter space that takes the shape of an airfoil

457 containing points suitable for surge-type glaciers. In all cases, these airfoil features are isolated from the
 458 main region of surging, oriented at roughly the same angles in the parameter space, have long-axes lengths
 459 that scale nonlinearly with ϵ_e/ϵ_p , and have positions that shift toward higher t_h and smaller b as ϵ_e/ϵ_p in-
 460 creases. The boundaries of these features are diffuse in the direction of smaller t_h and b but feature sharp
 461 transitions in both max and final slip rates at higher t_h and b values. Second, the boundary separating the
 462 surging region from the non-surging and abandoned surge regions is sharp, rather than diffuse, suggesting
 463 the existence of a supercritical Hopf bifurcation at the (approximately) linear boundary between surging and
 464 non-surging in the t_h - b parameter space. As expounded on in the Discussion section, this sharp boundary
 465 and possible bifurcation illuminates some potential mechanisms that cause surging to switch on and off over
 466 longer (multi-centennial) timescales in given glacier system, and for surging glaciers to be relatively rare
 467 and geographically clustered. We reserve for future work detailed exploration of bifurcations in the system.

468 To better understand the features in Fig. 5, we further explore the dynamics in Fig. 6, which shows that
 469 small variations in b for fixed values of t_h and ϵ_e/ϵ_p lead to a range of responses. The parameter values repre-
 470 sented in Fig. 6 are shown with corresponding colors in Fig. 5. In order of decreasing b , we observe surging
 471 following the perturbation (blue line; $b = 0.03$), abandoned surging (orange line; $b = 0.028$), an abandoned
 472 surge followed by a surge at longer timescales (red line; $b = 0.026$), and slight dynamical variations (green
 473 and olive lines; $b \leq 0.024$). These transitions in dynamical behavior as a function of decreasing b can be
 474 understood in the context of changes in μ , the internal friction coefficient of the till. The sensitivity of μ to
 475 changes in state increases with b values, allowing for greater and more rapid reductions in the friction coef-
 476 ficient — and, by extension, the shear strength of the till, τ_t (lowest panel of 6) — at higher b values. Thus,
 477 higher b values lead to unstable acceleration immediately following the perturbation by allowing dynamic
 478 glacier thinning driven a net reduction in the effective pressure, further decreasing the shear strength of the
 479 till. Slightly smaller b values in the abandoned surge region result in slightly smaller changes in μ , which
 480 creates a situation that is unfavorable to surging because the acceleration in basal slip rate is sufficiently fast
 481 to drive till evolution but not significant dynamic thinning of the glacier. As a result, the initial acceleration
 482 is facilitated by reductions in both the effective pressure and internal friction coefficient, but decreases in
 483 pore water pressure eventually outpace reductions in overburden pressure, resulting in an net increase in
 484 effective pressure (and τ_t) and ultimate stagnation of basal slip. Finally, a delayed surge manifests at median
 485 b values ($b = 0.026$ for $t_h = 2600$ days; red line in Fig. 6) due to trade-offs in basal slip acceleration, till
 486 dilation, and evolution of the internal friction coefficient. In this case, small initial decreases in μ driven
 487 by state evolution allow for basal slip acceleration, which drives the till toward steady state and ultimately
 488 increases state beyond the initial steady state value as the glacier slows. Since basal slip does not stagnate
 489 as it did in the previously discussed case, the till continues to evolve, eventually leading to compaction and
 490 commensurate increase in pore water pressure. This increase in pore water pressure drives a reduction in
 491 effective pressure that leads to glacier acceleration, which eventually becomes self-sustaining as the glacier
 492 thins and effective pressure drops.

493 We find good agreement between our model behavior and observations of surge motion in natural
 494 glaciers (Fig. 7). Our model reproduces both the timing and order of magnitude of the speedup with a
 495 range of values for the evolution coefficient b and diffusion timescale t_h . In Fig. 7 we show results using
 496 $b = 0.03$ and $t_h = 3000$ days and other parameters corresponding to values used in Figs. 3 and 4. Note
 497 that our focus in this study has been on the incipient acceleration phase of the surges, and simplifications in
 498 the model, namely the lack of an evolving subglacial hydrological system and consideration of extensional
 499 stresses in the momentum balance, prevent the model from decelerating [10]. The agreement between our
 500 model and these data, however, is encouraging as it suggests that the dilation and glacier-thinning timescales
 501 we consider in our model do indeed work in concert to trigger glacier surges.

502 4 Discussion

503 At this point, we have derived and explored the behavior of a fundamentally new dynamical model of
504 incipient surge motion that considers the mechanics of subglacial till and ice flow. Few comparable models
505 exist in the literature, thus we endeavor to develop the simplest model capable of capturing the salient
506 physical processes of ice slipping due to deformation of beds composed of water-saturated till. As detailed
507 later in this section, natural glacier systems will, of course, be more complex than our model. Nevertheless,
508 our model evinces rich dynamical behaviors consistent with observations, suggesting that our model strikes
509 an appropriate balance between capturing the salient physical processes while remaining simple enough to
510 allow for physical insight.

511 4.1 Mechanics of incipient surge motion

512 Rich dynamical behavior in our model is driven by the interactions of the three factors that define the shear
513 strength of the till $\tau_t = (p_i - p_w)\mu$: the overburden pressure $p_i = \rho_i gh$, pore water pressure p_w , and
514 the rate-and-state-dependent internal friction coefficient $\mu = \mu(u_b, \theta)$. To understand surge behavior in
515 glaciers with till-covered beds, it is important to recognize that pore water pressure tends to decrease due to
516 dilation, which strengthens till and resists surge motion, while the internal friction coefficient can increase
517 or decrease, often by small amounts. Rate-weakening internal friction ($a - b < 0$) can help to facilitate
518 surges but is not a necessary condition as surges are possible with rate-strengthening friction coefficients
519 ($a - b > 0$) under conditions that allow for reduction in effective pressure (Fig. 5).

520 The key process governing incipient surge motion is suction caused by till dilation in relatively imper-
521 meable till. In this case, pore water pressure decreases in response to shear-driven dilation, and the drop in
522 pore water pressure diminishes the ability of till to evolve to a new steady state. If hydraulic permeability
523 is sufficiently low (*i.e.*, if the diffusion time of the deforming till layer t_h is sufficiently long), slowing of
524 state evolution allows the glacier to accelerate for longer periods of time. This longer acceleration phase
525 gives the glacier time to thin dynamically, which reduces the overburden pressure (p_i). In the region of the
526 parameter space shown in Fig. 5, the reduction in overburden pressure outpaces drops in pore water pressure
527 (p_w) leading to a net reduction in the effective pressure ($N = p_i - p_w$) and thereby the shear strength of till
528 ($\tau_t = \mu N$). From Eqs. 24 and 32, we can see that the rate of change in driving stress is $\dot{\tau}_d \approx 2\dot{p}_i\alpha$, indicat-
529 ing that driving stress evolves at least an order of magnitude more slowly than changes in overburden due
530 to the shallow slopes of glaciers ($\alpha \ll 1$). As a result, reductions in overburden pressure facilitate sustained
531 excess driving stress ($\tau_d > \tau_b$), the key ingredient for sustained incipient surge motion. It is necessary, then,
532 that the initial acceleration must be large enough and last for long enough to generate sufficient dynamical
533 thinning of the glacier.

534 4.2 Implications of surge mechanics

535 The need for dynamic thinning to sustain surge motion gives two necessary conditions for glacier surging:
536 till must have sufficiently low hydraulic permeability to allow for incipient surge motion to be maintained
537 over a long enough period of time, and the velocity during the nascent surge must exceed the balance
538 velocity to allow for dynamical thinning. The latter condition implies a third necessary condition: shear
539 strength of the till must be less than the balance driving stress, defined as the driving stress at which the
540 balance velocity is achieved through internal deformation of the ice column. Consequently, yielding of the
541 till must occur at glacier velocities slower than the balance velocity to allow for continual shear-loading of
542 the till.

543 In the accumulation zones of surging glaciers, flow speeds must be slower than the balance velocity to
544 build an ever-thickening reservoir of ice [15]. This condition must persist throughout the quiescent phase

545 because once the flow speed reaches the balance velocity, there would be no way to further increase driving
546 stress and load the bed as ice-mass would be evacuated by flow accommodated through vertical shearing of
547 the ice column. In other words, mass balance along with the geometric and rheological properties of surge-
548 type glaciers allow them to build a reservoir that exerts a driving stress equal to bed failure strength before
549 flow rates reach the balance velocity. To illustrate this point, consider that the maximum load a glacier can
550 apply to its bed is given by the gravitational driving stress when the surface velocity of the ice equals the
551 balance velocity and basal slip rate is negligible ($\tau_b \approx \tau_d$). Surface velocity due solely to vertical shearing
552 within the ice column u_v is given by assuming that stress increases linearly with depth, that ice rheology is
553 constant with depth, and that ice flow is parallel to the ice surface, yielding

$$u_v = \frac{2Ah\tau_d^n}{n+1}, \quad (33)$$

554 where A is the prefactor and n is the stress exponent in the constitutive relation for ice (Eq. 25). Defining
555 the rate of change in driving stress as (cf. Eqs. 24, 31, and 32)

$$\dot{\tau}_d \approx 2\rho_i g \alpha^2 \zeta (u_* - u_s), \quad (34)$$

556 and setting $u_s = u_v = u_*$ in Eq. 34 gives the balance driving stress

$$\tau_{d*} = \tilde{\tau}_d \left(\frac{n+2}{2} \right)^{\frac{1}{n+1}} \approx 1.25 \tilde{\tau}_d, \quad (35)$$

557 where the potential drag at the bed is

$$\tilde{\tau}_d = \left(\frac{\rho_i g \dot{M}}{A} \right)^{\frac{1}{n+1}}, \quad (36)$$

558 whose variables \dot{M} , A , and, to a lesser extent, ρ_i are governed by local climate [90]. Although mass density
559 cannot vary more than 25%, \dot{M} and A can vary independently by orders of magnitude. Thus, potential drag
560 $\tilde{\tau}_d$ for an idealized glacier is determined almost exclusively by \dot{M}/A , the ratio of mass balance, \dot{M} , to the rate
561 factor, A , which depends on ice temperature and interstitial meltwater content, along with crystallographic
562 fabric [99].

563 Eqs. 35 and 36 underpin a necessary condition for surging: At a minimum, surging glaciers must
564 have a climate, and geometry, that allows for sufficiently high $\tilde{\tau}_d$ values—a combination of high mass
565 balance and stiff ice (i.e. small A)—to overcome the strength of their beds. As a result, the geographic
566 distribution of surge-type glaciers will reflect areas that combine sufficiently high rates of snowfall, relatively
567 low summertime melt at the surface, and cold, stiff ice with beds that have yield stresses below the respective
568 $\tilde{\tau}_d$ but are strong enough to allow the glacier to develop driving stresses that allow for order-of-magnitude
569 increases in ice flow during the surge. Assuming that the pre-surge surface velocity, $u_{s_{pre}}$, in the region
570 where a surge begins is primarily due to viscous deformation in the ice column (i.e., $\tau_{b_{pre}} \approx \tau_{d_{pre}}$) and
571 considering that surface velocity at peak surge speeds, $u_{s_{surge}}$, is due primarily to basal slip, the gravitational
572 driving stress necessary to produce a given speedup can be approximated as

$$\tau_{d_{pre}} \approx \tau_{t_{surge}} \left[1 - \frac{u_{s_{surge}} h_{surge}^n h_{pre}}{u_{s_{pre}} w^{n+1}} \right]^{-1/n}, \quad (37)$$

573 where $\tau_{t_{surge}}$ is the shear strength of the till when the glacier is flowing at peak surge speed. Note that
574 typical values for the bracketed term in Eq. 37 will be approximately one for glaciers that are wider than
575 they are thick (a condition stated at the beginning of the model derivation). Combining Eq. 37 with the
576 balance velocity explicitly gives the necessary condition

$$\tau_{d_{pre}} < \tau_{d*}, \quad (38)$$

577 which to a good approximation is simply $\bar{\tau}_t < \bar{\tau}_d$, where $\bar{\tau}_t$ is the long-term average shear strength of
578 the till in the region where surges nucleate. The range of reasonable values on $\rho_i g$ is small, so to a good
579 approximation, whether a glacier meets the condition in Eq. 38 is determined primarily by mass balance,
580 ice rheology, bed strength, and cross-sectional aspect ratio (h/w).

581 The condition defined by Eqs. 35 through 38 yield surge conditions discussed in previous observa-
582 tional studies. The dependence on mass balance is consistent with observations that have shown cumulative
583 quiescent-phase mass balance to be a reliable predictor of surging on Variegated Glacier, Alaska [100, 101].
584 The temperature-dependent ice rheology reproduces the climatic and geometric trends reported in [12] (Fig.
585 8). In this framework, warmer climate (and ice temperatures) require higher values of surface mass balance
586 to satisfy the condition that the bed yields before the driving stress becomes high enough to cause the glacier
587 to flow at the balance velocity through internal deformation within the ice.

588 Further insight into the spatial distribution and longer-term evolution of surge-type glaciers can be
589 gleaned from the boundaries between surge-type and non-surge-type glaciers illuminated in the permeability
590 vs evolution effect parameter space (Fig. 5). The sharp, diagonal boundary between surging on non-surge
591 behavior suggests the existence of a Hopf bifurcation in the system and lies at values that are likely to be
592 relatively rare in nature and closely linked to local lithology and degree of weathering. In particular, our
593 model suggests that values of hydraulic diffusivity for till in surge-type glaciers falls in the lower range of
594 observed values ($\sim 10^{-9}$ m²/s) for the range of b values explored in this study. Such low hydraulic dif-
595 fusivities are consistent with canonical values of permeability expected for fine-grain sediments and loams
596 [58, 90]. The need for such low values of hydraulic permeability and fine-grained sediments suggests a
597 potential role for comminution and sediment transport in activating and deactivating surging over millennial
598 timescales, though future work is needed to elucidate these connections.

599 The governing role of till dilation and evolving pore water pressure in our model points to further meth-
600 ods for testing the model in nature. In addition to the comparisons with data similar to those given in this
601 study (namely Fig. 7 and the preceding discussion of geographic distribution of surge-type glaciers), we
602 propose that passive seismic data collected during the incipient surge phase would provide valuable insight
603 into the salient processes and could be used to test our model. Passive seismic data are routinely used to
604 estimate the seismic moment from which estimates of the bulk shear modulus can be gleaned. The shear
605 modulus is sensitive to both the porosity and pore water pressure, and so can be used as a means to observe
606 till dilation and variations in pore water pressure.

607 **4.3 Model limitations and future development**

608 Our goal with this work is to better understand basal mechanics by developing a model for incipient surge
609 motion in glaciers with till-covered beds. We do not attempt to capture all of the processes that may be
610 important in initiating and sustaining glacier surges. As a result, our model has some limitations that provide
611 avenues for future work.

612 A notable limitation is the lack of explicit treatment for evolution of the subglacial hydrological system
613 during any stage of the surge or the quiescent phase. The influence of basal hydrological characteristics is
614 manifested in the model through the system water pressure $p_{w,r}$, but we implicitly treat this water pressure
615 as passive in the model development. A fully passive basal hydrological system is unlikely given the rapid,
616 extreme changes in glacier dynamics that define a surge. During surges, significant volumes of till are
617 displaced, filling most existing cavities, basal crevasses, or channels that constitute the contemporaneous
618 hydrological system [17]. This lack of explicit treatment for changes in $p_{w,r}$ due to till displacement leaves
619 open the possibility that increases in basal water pressure caused by changes in the basal hydrological
620 system can cause surges. What we have provided in this study are proposed mechanisms of incipient surge
621 motion in glaciers with deformable beds that are not dependent on changes in the basal hydrological system.
622 The existence of such a mechanism, which works equally well for temperate and polythermal glaciers, and

623 observations of surges beginning in times of the year when there is little or no additional surface meltwater
624 available to pressurize a basal hydrological system (e.g. during winter), supports the hypothesis that it is the
625 incipient surge motion that diminishes the efficiency of any extant hydrological system rather than changes
626 in the hydrological system that lead to surges.

627 We do not explicitly consider enhanced melting of basal ice through frictional heating or viscous dis-
628 sipation. The reason for this exclusion is twofold. First, melt-rates scale linearly with the product of basal
629 slip rate and till shear strength. While this product likely increases during the early surge phase, the trade-
630 off between diminished till shear strength, basal slip rate, and the characteristics of subglacial hydrological
631 systems is nontrivial and leads to melt rates that are orders of magnitude below surface meltwater fluxes in
632 many areas [30, 59]. The second reason we exclude slip-induced melting is that melting only influences ice
633 dynamics through changes in basal and pore water pressure [10]. Without a reliable model for subglacial
634 hydrology, there is no way to effectively link basal melt rate and water pressure.

635 Our model does not capture the down-glacier propagation of mechanical, kinematic, or basal-water
636 pressure waves [19, 102]. This limitation arises from the fact that our model is essentially one-dimensional,
637 meaning that we neglect extensional (along-flow normal) stresses and strain rates (Eqs. 26 and 31) along
638 with horizontal gradients in water pressure. During the quiescent phase, neglecting extensional stresses is
639 reasonable in the upper accumulation zone where surges are prone to begin. Here, surface velocities tend
640 to be slow and relatively consistent over large spatial scales, meaning that along-flow strain rates are small
641 relative to the effective strain rate; since ice is a viscous fluid, low strain rates mean low stresses. During
642 the surge, the surface velocities are high, with the exception of the period when surge waves are present,
643 and velocities can be expected to have small spatial gradients [6, 27]. A more complete model of glacier
644 surges would include more terms of the stress divergence such that it could account for the propagation of
645 surge motion through the glacier. This more complete model would be useful for further investigating the
646 influence of glacier length on surge behavior [10]. However, we consider our box-model analysis to be a
647 prerequisite to more complicated flowline and 3D studies, which we reserve for future work.

648 **5 Summary and Conclusions**

649 In this paper, we develop a new model of incipient surge motion in glaciers with till covered beds. Incipient
650 surge motion in our model occurs in the absence of enhanced water flux to the bed, changes to the basal
651 hydrological system, and freeze-thaw cycles in till. Our model is based on granular mechanics of the till
652 and focuses on processes that can lead to unstable acceleration in glaciers with deformable beds. Our
653 model is unique among existing surge models in that it accounts for till porosity and pore water pressure,
654 and represents the evolution of internal friction, porosity, and pore water pressure within the deforming till
655 layer as a functions of the rate and history of shearing within the deforming till layer. This combination
656 of mechanisms allows for exploration of the rich dynamics that arise from changes in the three factors
657 that govern the shear strength of till: ice overburden pressure, pore water pressure, and the internal friction
658 coefficient. To represent these factors, we adopt the phenomenological rate-and-state model commonly used
659 in studies of slip on tectonic faults. We link the state variable, which encodes the history of basal slip, to till
660 porosity and derive a model in which pore water pressure evolves due to changes in porosity and transport
661 of pore water (*i.e.*, Darcy flow) into and out of the deforming till layer.

662 We find that till dilation, and more specifically suction caused by the reduction of pore water pressure
663 in response to dilation, is a fundamental control on incipient surge motion. This control arises from the
664 need for dynamic thinning of the glacier to sustain surge motion by reducing the effective pressure at the
665 bed. Glacier thinning is necessary because, following a perturbation, till tends toward a new steady state
666 while flow of water into and out of the deforming layer acts to equalize pore water pressure between the
667 underlying static till layer, the deforming till layer, and the subglacial hydrological system. As a result,
668 the shear strength of the bed tends to a new steady state, leading to stable acceleration, unless the glacier

669 thins. If the permeability of the till is sufficiently low, the evolution of the till to a new steady state is slow
670 enough to allow accelerated surge motion to thin the glacier, so long as flow speeds during the nascent surge
671 exceed the glacier's balance velocity. Thinning of the glacier allows for unstable acceleration of the glacier
672 due to reductions in shear strength of the till, leading to order-of-magnitude increases in flow velocity that
673 characterize surges and are consistent with observations of glacier acceleration during surges.

674 The hydromechanical properties of till, namely the need for low till permeability, required to induce
675 rapid glacier thinning and surge motion give rise to restrictive conditions for glacier surges and rich dynam-
676 ics. The necessary conditions for surging illuminated by our model are low hydraulic permeability in the
677 deforming till layer, surge velocities that exceed the balance velocity, and maximum shear strength of till
678 that is less than the driving stress needed to achieve the balance velocity through vertical shearing in the ice
679 column. These conditions are consistent with the rarity of surge-type glaciers; the geographic and climatic
680 distribution and clustering of surge-type glaciers; and millennial-timescale evolution of surge behavior. Fur-
681 thermore, the rich dynamics produced by our model allow for abandoned surges along with a spectrum of
682 surge-like behaviors that are consistent with kinematic observations of natural glaciers but are lacking in
683 existing surge models.

684 Our model is necessarily simplified but contains important new physical processes — namely, till me-
685 chanics — that have been neglected in virtually all previous studies of glacier surges. To focus on the
686 complex processes of water saturated till, we deliberately ignore other processes that may be essential for a
687 complete understanding of surge dynamics. Most notably, we neglect extensional stresses and vertical shear-
688 ing in the ice column, and we treat the subglacial hydrological system as static. As a result, our model only
689 captures the incipient surge phase and not slowdowns that terminate surges. We derive our model such that
690 the inclusion of a dynamic subglacial hydrological system should be a relatively straightforward additions
691 and extension and vertical shear stresses can be included with the application of a more sophisticated flow
692 model that accounts for more terms of the stress divergence in the momentum equations. These avenues
693 provide numerous opportunities for future exploration of surge dynamics.

694 *Data access:* No new data are presented in this study. Source code for the numerical simulations is available
695 at github.com/bminchew/glacier_surging1.git.

696 *Author contribution:* BM conceived the project, led the model development, and drafted the manuscript.
697 CM provided essential insight, assisted with model development, and helped revise the manuscript.

698 *Competing Interests:* The authors declare no competing interests.

699 *Funding:* At various stages of this work, B.M. was partially funded by a NASA Cyospheric Sciences award
700 NNX14AH80G, generous donations from the Albert Parvin and ARCS LA Chapter foundations, and an
701 NSF Earth Science Postdoctoral Fellowship award EAR-1452587. C.M. acknowledges support from the
702 David Crighton Fellowship, NSF-1144152 and NSF-1603907.

703 *Acknowledgements:* We thank James Rice, Alan Rempel, Bradley Lipovsky, Lucas Zoet, and Robert Viesca
704 for insightful discussions.

705 **References**

706 [1] M. F. Meier and A. Post. What are glacier surges? *Canadian Journal of Earth Sciences*, 6(4):
707 807–817, 1969.

708 [2] C. Raymond. How do glaciers surge? A review. *Journal of Geophysical Research*, 92(B9):9121–
709 9134, 1987. doi: 10.1029/JB092iB09p09121.

710 [3] B. Kamb. Glacier surge mechanisms based on linked cavity configuration of the basal water conduit
711 system. *Journal of Geophysical Research*, 92(B9):9083–9100, 1987.

712 [4] T. Murray, G. W. Stuart, P. J. Miller, J. Woodward, A. M. Smith, P. R. Porter, and H. Jiskoot. Glacier
713 surge propagation by thermal evolution at the bed. *Journal of Geophysical Research: Solid Earth*,
714 105(B6):13491–13507, 2000. doi: 10.1029/2000JB900066.

715 [5] A. C. Fowler, T. Murray, and F. S. L. Ng. Thermally controlled glacier surging. *Journal of Glaciology*,
716 47(159):527–538, 2001.

717 [6] T. Murray, T. Strozzi, A. Luckman, H. Jiskoot, and P. Christakos. Is there a single surge mechanism?
718 Contrasts in dynamics between glacier surges in Svalbard and other regions. *Journal of Geophysical
719 Research*, 108(B5):1–15, 2003. doi: 10.1029/2002JB001906. 2237.

720 [7] G. E. Flowers, N. Roux, S. Pimentel, and C. G. Schoof. Present dynamics and future prognosis of a
721 slowly surging glacier. *The Cryosphere*, 5:299–313, 2011. doi: 10.5194/tc-5-299-2011.

722 [8] C. R. Meyer, M. C. Fernandes, T. T. Creyts, and J. R. Rice. Effects of ice deformation on Røthlisberger
723 channels and implications for transitions in subglacial hydrology. *Journal of Glaciology*, 62(234):
724 750–762, 2016. doi: 10.1017/jog.2016.65.

725 [9] G. E. Flowers, A. H. Jarosch, P. T. A. P. Belliveau, and L. A. Fuhrman. Short-term velocity variations
726 and sliding sensitivity of a slowly surging glacier. *Annals of Glaciology*, 57(72):71–83, 2016. doi:
727 10.1017/aog.2016.7.

728 [10] D. I. Benn, A. C. Fowler, I. Hewitt, and H. Sevestre. A general theory of glacier surges. *Journal of
729 Glaciology*, 65(253):701–716, 2019. doi: 10.1017/jog.2019.62.

730 [11] H. Jiskoot, P. Boyle, and T. Murray. The incidence of glacier surging in Svalbard: evidence from
731 multivariate statistics. *Computational Geoscience*, 24(4):387–399, 1998.

- 732 [12] H Sevestre and D I Benn. Climatic and geometric controls on the global distribution of surge-type
733 glaciers: implications for a unifying model of surging. *Journal of Glaciology*, 61(228):646–662,
734 2015.
- 735 [13] H. Jiskoot, T. Murray, and P. Boyle. Controls on the distribution of surge-type glaciers in Svalbard.
736 *Journal of Glaciology*, 46(154):412–422, 2000.
- 737 [14] M. Truffer, W. D. Harrison, and K. A. Echelmeyer. Glacier motion dominated by processes deep in
738 underlying till. *Journal of Glaciology*, 46(153):213–221, 2000. doi: 10.3189/172756500781832909.
- 739 [15] H. Björnsson, F. Pálsson, O. Sigurðsson, and G. Flowers. Surges of glaciers in Iceland. *Annals of*
740 *Glaciology*, 36:82–90, 2003. doi: 10.3189/172756403781816365.
- 741 [16] W. D. Harrison and A. S. Post. How much do we really know about glacier surging? *Annals of*
742 *Glaciology*, 36:1–6, 2003.
- 743 [17] J. Woodward, T. Murray, R. A. Clark, and G. W. Stuart. Glacier surge mechanisms inferred from
744 ground-penetrating radar: Kongsvegen, Svalbard. *Journal of Glaciology*, 49(167):473–480, 2003.
745 doi: 10.3189/172756503781830458.
- 746 [18] A. Fowler. *Mathematical Geoscience*. Springer, London, 2011.
- 747 [19] B. Kamb, C. F. Raymond, W. D. Harrison, H. Engelhardt, K. A. Echelmeyer, N. Humphrey, M. M.
748 Brugman, and T. Pfeffer. Glacier surge mechanism: 1982-1983 surge of Variegated Glacier, Alaska.
749 *Science*, 227(4686):469–479, 1985. doi: 10.1126/science.227.4686.469.
- 750 [20] H. Björnsson. Hydrological characteristics of the drainage system beneath a surging glacier. *Nature*,
751 395(6704):771–774, 1998. doi: 10.1038/27384.
- 752 [21] Hamish Pritchard, Tavi Murray, Adrian Luckman, T Strozzi, and Stuart Barr. Glacier surge dynamics
753 of Sortebræ, east Greenland, from synthetic aperture radar feature tracking. *Journal of Geophysical*
754 *Research*, 110(F03005):1–13, 2005. doi: 10.1029/2004JF000233.
- 755 [22] Douglas I. Benn, Lene Kristensen, and Jason D. Gulley. Surge propagation constrained by a persis-
756 tent subglacial conduit, Bakaninbreen-Paulabreen, Svalbard. *Annals of Glaciology*, 50(52):81–86,
757 2009. doi: 10.3189/172756409789624337.
- 758 [23] V. Round, S. Leinss, M. Huss, C. Haemmig, and I. Hajnsek. Surge dynamics and lake outbursts of
759 Kyagar Glacier, Karakoram. *The Cryosphere*, 11(2):723–739, 2017. doi: 10.5194/tc-11-723-2017.
- 760 [24] K. Echelmeyer, R. Butterfield, and D. Cuillard. Some observations on a recent surge of Peters Glacier,
761 Alaska, U.S.A. *Journal of Glaciology*, 33(115):341–345, 1987.
- 762 [25] J. J. Roush, C. G. Lingle, R. M. Guritz, D. R. Fatland, and V. A. Voronina. Surge-front propagation
763 and velocities during the early 1993–1995 surge of Bering Glacier, Alaska, U.S.A., from sequential
764 SAR imagery. *Annals of Glaciology*, 36:37–44, 2003.
- 765 [26] A. Bevington and L. Copland. Characteristics of the last five surges of Lowell Glacier, Yukon,
766 Canada, since 1948. *Journal of Glaciology*, 60(219):113–123, 2014. doi: 10.3189/2014JoG13J134.
- 767 [27] T. Dunse, T. Schellenberger, J. O. Hagen, A. Käab, T. V. Schuler, and C. H. Reijmer. Glacier-surge
768 mechanisms promoted by a hydro-thermodynamic feedback to summer melt. *The Cryosphere*, 9:
769 197–215, 2015. doi: 10.5194/tc-9-197-2015.

- 770 [28] G. de Q. Robin. Ice movement and temperature distribution in glaciers and ice sheets. *Journal of*
771 *Glaciology*, 2(18):523–532, 1955.
- 772 [29] D. R. MacAyeal. Binge/purge oscillations of the laurentide ice sheet as a cause of the north atlantic’s
773 heinrich events. *Paleoceanography*, 8(6):775–784, 1993. doi: 10.1029/93PA02200.
- 774 [30] A. A. Robel, E. DeGiuli, C. Schoof, and E. Tziperman. Dynamics of ice stream temporal variability:
775 Modes, scales, and hysteresis. *Journal of Geophysical Research: Earth Surface*, 118(2):925–936,
776 2013. doi: 10.1002/jgrf.20072.
- 777 [31] C. R Meyer, A. A Robel, and A. W Rempel. Frozen fringe explains sediment freeze-
778 on during heinrich events. *Earth and Planetary Science Letters*, 524:115725, 2019. doi:
779 10.1016/j.epsl.2019.115725.
- 780 [32] G. K. C. Clarke. Thermal regulation of glacier surging. *Journal of Glaciology*, 16(74):231–250,
781 1976.
- 782 [33] G. K. C. Clarke, U. Nitsan, and W. S. B. Paterson. Strain heating and creep instability in glaciers and
783 ice sheets. *Reviews of Geophysics and Space Physics*, 15(2):235–247, 1977.
- 784 [34] M. Sund, T. R. Lauknes, and T. Eiken. Surge dynamics in the Nathorstbreen glacier system, Svalbard.
785 *The Cryosphere*, 8:623–638, 2014. doi: 10.5194/tc-8-623-2014.
- 786 [35] N. J. Wilson, G. E. Flowers, and L. Mingo. Mapping and interpretation of bed-reflection power from
787 a surge-type polythermal glacier, Yukon, Canada. *Annals of Glaciology*, 55(67):1–8, 2014. doi:
788 10.3189/2014AoG67A101.
- 789 [36] K. Thøgersen, A. Gilbert, T. V. Schuler, and A. Malthe-Sørenssen. Rate-and-state friction explains
790 glacier surge propagation. *Nature Communications*, 10(2823):1–8, 2019. doi: 10.1038/s41467-019-
791 10506-4.
- 792 [37] G. K. C. Clarke. Subglacial till: A physical framework for its properties and processes. *Journal of*
793 *Geophysical Research: Solid Earth*, 92(B9):9023–9036, 1987. doi: 10.1029/JB092iB09p09023.
- 794 [38] A. W. Rempel. A theory for ice-till interactions and sediment entrainment beneath glaciers. *Journal*
795 *of Geophysical Research*, 113:1–20, 2008. doi: 10.1029/2007JF000870. F01013.
- 796 [39] L. K. Zoet, B. Carpenter, M. Scuderi, R. B. Alley, S. Anandakrishnan, C. Marone, and M. Jackson.
797 The effects of entrained debris on the basal sliding stability of a glacier. *Journal of Geophysical*
798 *Research: Earth Surface*, 118(2):656–666, 2013. doi: 10.1002/jgrf.20052.
- 799 [40] C. R. Meyer, A. S. Downey, and A. W. Rempel. Freeze-on limits bed strength beneath sliding glaciers.
800 *Nature Communications*, 9(3242):1–6, 2018. doi: 10.1038/s41467-018-05716-1.
- 801 [41] L. K. Zoet and N. R. Iverson. Rate-weakening drag during glacier sliding. *Journal of Geophysical*
802 *Research: Earth Surface*, 121(7):1206–1217, 2016. doi: 10.1002/2016JF003909.
- 803 [42] Lucas K. Zoet and Neal R. Iverson. A healing mechanism for stick-slip of glaciers. *Geology*, 46(9):
804 807–810, 2018. doi: 10.1130/G45099.1.
- 805 [43] J. F. Thomason and N. R. Iverson. A laboratory study of particle ploughing and pore-pressure feed-
806 back: a velocity-weakening mechanism for soft glacier beds. *Journal of Glaciology*, 54(184):169–
807 181, 2008. doi: 10.3189/002214308784409008.

- 808 [44] N. R. Iverson, R. G. McCracken, L. K. Zoet, Í. Ö. Benediktsson, A. Schomacker, M. D. John-
809 son, and J. Woodard. A theoretical model of drumlin formation based on observations at Múla-
810 jökull, Iceland. *Journal of Geophysical Research: Earth Surface*, 122(12):2302–2323, 2017. doi:
811 10.1002/2017JF004354.
- 812 [45] R. O. Davis and A. P. S. Selvadurai. *Plasticity and Geomechanics*. Cambridge University Press,
813 Cambridge, England, first edition, 2002.
- 814 [46] A. Fowler. On the rheology of till. *Annals of Glaciology*, 37:55–59, 2003. doi:
815 10.3189/172756403781815951.
- 816 [47] M. Truffer, K. A. Echelmeyer, and W. D. Harrison. Implications of till deformation on glacier dy-
817 namics. *Journal of Glaciology*, 47(156):123–134, 2001. doi: 10.3189/172756501781832449.
- 818 [48] P. L. Moore and N. R. Iverson. Slow episodic shear of granular materials regu-
819 lated by dilatant strengthening. *Geology*, 30(9):843–846, 2002. doi: 10.1130/0091-
820 7613(2002)030<0843:SESOGM>2.0.CO;2.
- 821 [49] J. H. Dieterich. Modeling of rock friction. Part 1: Experimental results and constitutive equations.
822 *Journal of Geophysical Research*, 84(B5):2161–2168, 1979. doi: 10.1029/JB084iB05p02161.
- 823 [50] A. Ruina. Slip instability and state variable friction laws. *Journal of Geophysical Research*, 88(B12):
824 10359–10370, 1983. doi: 10.1029/JB088iB12p10359.
- 825 [51] B. Kamb. Rheological nonlinearity and flow instability in the deforming-bed mechanism of ice
826 stream motion. *Journal of Geophysical Research: Solid Earth*, 96(B10):16585–16595, 1991. doi:
827 10.1029/91JB00946.
- 828 [52] B. D. Kilgore, J. H. Dieterich, and M. L. Blanpied. Velocity dependent friction of granite over a wide
829 range of conditions. *Geophysical Research Letters*, 20(10):903–906, 1993. doi: 10.1029/93GL00368.
- 830 [53] N. R. Iverson, T. S. Hooyer, and R. W. Baker. Ring-shear studies of till deformation: Coulomb plastic
831 behavior and distributed strain in glacier beds. *Journal of Glaciology*, 44:634–642, 1998.
- 832 [54] S. Tulaczyk, W. B. Kamb, and H. F. Engelhardt. Basal mechanics of Ice Stream B, west Antarctica:
833 1. Till mechanics. *Journal of Geophysical Research: Solid Earth*, 105(B1):463–481, 2000. doi:
834 10.1029/1999JB900329.
- 835 [55] R. LeB. Hooke. *Principles of Glacier Mechanics*. Cambridge University Press, New York, NY,
836 second edition, 2005.
- 837 [56] N. R. Iverson. Shear resistance and continuity of subglacial till: hydrology rules. *Journal of Glaciol-*
838 *ogy*, 56(200):1104–1114, 2010. doi: 10.3189/002214311796406220.
- 839 [57] N. R. Iverson and L. K. Zoet. Experiments on the dynamics and sedimentary products of glacier slip.
840 *Geomorphology*, 244:121–134, 2015. doi: 10.1016/j.geomorph.2015.03.027.
- 841 [58] T. W. Lambe and R. V. Whitman. *Soil Mechanics*. Wiley, New York, NY, 1969.
- 842 [59] S. Tulaczyk, W. B. Kamb, and H. F. Engelhardt. Basal mechanics of Ice Stream B, west Antarctica:
843 2. Undrained plastic bed model. *Journal of Geophysical Research: Solid Earth*, 105(B1):483–494,
844 2000. doi: 10.1029/1999JB900328.

- 845 [60] S. Fuller and T. Murray. Sedimentological investigations in the forefield of an Icelandic surge-type
846 glacier: implications for the surge mechanism. *Quaternary Science Reviews*, 21:1503–1520, 2002.
- 847 [61] A A Robel, Christian G Schoof, and E Tziperman. Rapid grounding line migration induced by
848 internal ice stream variability. *Journal of Geophysical Research: Earth Surface*, 119(11):2430–2447,
849 2014. doi: 10.1002/2014JF003251.
- 850 [62] A. A. Robel, C. Schoof, and E. Tziperman. Persistence and variability of ice-stream grounding lines
851 on retrograde bed slopes. *The Cryosphere*, 10(4):1883–1896, 2016. doi: 10.5194/tc-10-1883-2016.
- 852 [63] C. Schoof. Ice-sheet accerleration driven by melt supply variability. *Nature*, 468(7325):803–806,
853 2010. doi: 10.1038/nature09618.
- 854 [64] I. J. Hewitt. Seasonal changes in ice sheet motion due to melt water lubrication. *Earth and Planetary
855 Science Letters*, 371–372:16–25, 2013. doi: 10.1016/j.epsl.2013.04.022.
- 856 [65] M. A. Werder, I. J. Hewitt, C. G. Schoof, and G. E. Flowers. Modeling channelized and distributed
857 subglacial drainage in two dimensions. *Journal of Geophysical Research: Earth Surface*, 118(4):
858 2140–2158, 2013. doi: 10.1002/jgrf.20146.
- 859 [66] L. Lliboutry. General theory of subglacial cavitation and sliding of temperate glaciers. *Journal of
860 Glaciology*, 7(49):21–58, 1968.
- 861 [67] B. Kamb. Sliding motion of glaciers: theory and observations. *Reviews of Geophysics*, 8(4):673–728,
862 1970.
- 863 [68] A. C. Fowler. Sliding with cavity formation. *Journal of Glaciology*, 33:255–267, 1987.
- 864 [69] C. Schoof. The effect of cavitation on glacier sliding. *Proceeding of the Royal Society of London.
865 Series A, Mathematical and Physical Sciences*, 461:609–627, 2005. doi: 10.1098/rspa.2004.1350.
- 866 [70] B. P. Lipovsky and E. M. Dunham. Slow-slip events on the Whillans Ice Plain, Antarctica, described
867 using rate-and-state friction as an ice stream sliding law. *Journal of Geophysical Research: Earth
868 Surface*, 122(4):973–1003, 2017. doi: 10.1002/2016JF004183. 2016JF004183.
- 869 [71] C. McCarthy, H. Savage, and M. Nettles. Temperature dependence of ice-on-rock friction at realistic
870 glacier conditions. *Philosophical Transactions of the Royal Society A: Mathematical, Physical and
871 Engineering Sciences*, 375(2086):1–18, 2017. doi: 10.1098/rsta.2015.0348.
- 872 [72] J. R. Rice. Constitutive relations for fault slip and earthquake instabilities. *Pure and Applied Geo-
873 physics PAGEOPH*, 121(3):443–475, 1983.
- 874 [73] P. Segall and J. R. Rice. Dilatancy, compaction, and slip instability of a fluid-infiltrated fault. *Journal
875 of Geophysical Research*, 100(B11):22155–22171, 1995. doi: 10.1029/95JB02403.
- 876 [74] P. Segall and J. R. Rice. Does shear heating of pore fluid contribute to earthquake nucleation? *Journal
877 of Geophysical Research*, 111(B09316):1–17, 2006. doi: 10.1029/2005JB004129.
- 878 [75] Jianye Chen, A R Niemeijer, and Christopher J Spiers. Microphysically Derived Expressions for
879 Rate-and-State Friction Parameters, a, b, and Dc. *Journal of Geophysical Research: Solid Earth*, 122
880 (12):9627–9657, 2017. doi: 10.1002/2017JB014226.

- 881 [76] A. P. Rathbun, C. Marone, R. B. Alley, and S. Anandkrishnan. Laboratory study of the fric-
882 tional rheology of sheared till. *Journal of Geophysical Research*, 113(F2):1–14, 2008. doi:
883 10.1029/2007JF000815. F02020.
- 884 [77] P. Segall, A. M. Rubin, A. M. Bradley, and J. R. Rice. Dilatant strengthening as a mecha-
885 nism for slow slip events. *Journal of Geophysical Research*, 115(B12305):1–37, 2010. doi:
886 10.1029/2010JB007449.
- 887 [78] J. H. Dieterich. Applications of rate- and state-dependent friction to models of fault slip and earth-
888 quake occurrence. In G. Schubert, editor, *Treatise on Geophysics*, pages 107–129. Elsevier, Amsterdam,
889 2007. doi: 10.1016/B978-044452748-6.00059-6.
- 890 [79] A C Palmer and James R Rice. The Growth of Slip Surfaces in the Progressive Failure of Over-
891 Consolidated Clay. *Proceedings of the Royal Society A: Mathematical, Physical and Engineering*
892 *Sciences*, 332(1591):527–548, 1973. doi: 10.1098/rspa.1973.0040.
- 893 [80] C. Marone and B. Kilgore. Scaling of the critical slip distance for seismic faulting with shear strain
894 in fault zones. *Nature*, 362(618):618–621, 1993. doi: 10.1038/362618a0.
- 895 [81] C. Marone, M. Cocco, E. Richardson, and E. Tinti. The critical slip distance for seismic and aseis-
896 mic fault zones of finite width. In *Fault-Zone Properties and Earthquake Rupture Dynamics*, vol-
897 ume 94 of *International Geophysics*, pages 135–162. Academic Press, 2009. doi: 10.1016/S0074-
898 6142(08)00006-5.
- 899 [82] A. Damsgaard, D. L. Egholm, J. A. Piotrowski, S. Tulaczyk, N. K. Larsen, and C. F. Brødstrup.
900 A new methodology to simulate subglacial deformation of water-saturated granular material. *The*
901 *Cryosphere*, 9(6):2183–2200, 2015. doi: 10.5194/tc-9-2183-2015.
- 902 [83] J.-P. Ampuero and A. M. Rubin. Earthquake nucleation on rate and state faults – aging and slip
903 laws. *Journal of Geophysical Research: Solid Earth*, 113(B1):n/a–n/a, 2008. ISSN 2156-2202. doi:
904 10.1029/2007JB005082. B01302.
- 905 [84] J. H. Dieterich and B. D. Kilgore. Direct observations of frictional contacts: New insights for sliding
906 memory effects. *Pure and Applied Geophysics*, 143:283–302, 1994.
- 907 [85] J. H. Dieterich. Constitutive properties of faults with simulated gouge. In N. L. Carter, M. Friedman,
908 J. M. Logan, and D. W. Stearns, editors, *Mechanical Behavior of Crustal Rocks: The Handin Volume*,
909 pages 103–120. American Geophysical Union, 1981. doi: 10.1029/GM024p0103.
- 910 [86] J. R. Rice and A. L. Ruina. Stability of Steady Frictional Slipping. *Journal of Applied Mechanics*, 50
911 (2):343–349, 06 1983. ISSN 0021-8936. doi: 10.1115/1.3167042.
- 912 [87] Joseph Walder and Amos Nur. Porosity reduction and crustal pore pressure development. *Journal of*
913 *Geophysical Research: Solid Earth*, 89(B13):11539–11548, 1984. doi: 10.1029/JB089iB13p11539.
- 914 [88] B. M. Minchew. *Mechanics of deformable glacier beds*. PhD thesis, California Institute of Technol-
915 ogy, 2016. Chapter 4, Appendix A.
- 916 [89] Neal R Iverson, Robert W Baker, and Thomas S Hooyer. A ring-shear device for the study of till
917 deformation: Tests on tills with contrasting clay contents. *Quaternary Science Reviews*, 16(9):1057–
918 1066, 1997. doi: 10.1016/S0277-3791(97)00036-X.
- 919 [90] K. M. Cuffey and W. S. B. Paterson. *The Physics of Glaciers*. Elsevier, 4th edition, 2010.

- 920 [91] G. S. Boulton and R. C. A. Hindmarsh. Sediment deformation beneath glaciers: Rheology and
921 geological consequences. *Journal of Geophysical Research: Solid Earth*, 92(B9):9059–9082, 1987.
922 doi: 10.1029/JB092iB09p09059.
- 923 [92] G.S. Boulton, K.E. Dobbie, and S. Zatsepin. Sediment deformation beneath glaciers and its
924 coupling to the subglacial hydraulic system. *Quaternary International*, 86(1):3–28, 2001. doi:
925 doi:10.1016/S1040-6182(01)00048-9.
- 926 [93] N. R. Iverson and R. M. Iverson. Distributed shear of subglacial till due to Coulomb slip. *Journal of*
927 *Glaciology*, 47(158):481–488, 2001.
- 928 [94] D. MacAyeal. Large-scale ice flow over a viscous basal sediment - Theory and application to Ice
929 Stream-B, Antarctica. *Journal of Geophysical Research*, 94(B4):4071–4087, 1989.
- 930 [95] B. M. Minchew, M. Simons, M. Morlighem, H. Björnsson, F. Pálsson, S. Hensley, and E. Larour.
931 Plastic bed beneath Hofsjökull Ice Cap, central Iceland, and the sensitivity of ice flow to surface
932 meltwater flux. *Journal of Glaciology*, 62(231):147–158, 2016. doi: 10.1017/jog.2016.26.
- 933 [96] J. W. Glen. The creep of polycrystalline ice. *Proceedings of the Royal Society of London A*, 228
934 (1175):519–538, 1955.
- 935 [97] Eric Jones, Travis Oliphant, Pearu Peterson, et al. SciPy: Open source scientific tools for Python,
936 2018. version 1.1.0.
- 937 [98] J. Mouginit, A. A. Bjørk, R. Millan, B. Scheuchl, and E. Rignot. Insights on the surge behavior of
938 storstrømmen and l. bistrup bræ, northeast greenland, over the last century. *Geophysical Research*
939 *Letters*, 45(11):11,197–11,205, 2018. doi: 10.1029/2018GL079052.
- 940 [99] B. M. Minchew, C. R. Meyer, A. A. Robel, G. H. Gudmundsson, and M. Simons. Processes con-
941 trolling the downstream evolution of ice rheology in glacier shear margins: Case study on Rutford Ice
942 Stream, West Antarctica. *Journal of Glaciology*, 64(246):583–594, 2018. doi: 10.1017/jog.2018.47.
- 943 [100] O. Eisen, W. D. Harrison, and C. F. Raymond. The surges of Variegated Glacier, Alaska, USA, and
944 their connection of climate and mass balance. *Journal of Glaciology*, 47(158):351–358, 2001.
- 945 [101] O. Eisen, W. D. Harrison, C. F. Raymond, K. A. Echelmeyer, G. A. Bender, and J. L. D. Gorda.
946 Variegated Glacier, Alaska, USA: a century of surges. *Journal of Glaciology*, 51(174):399–406,
947 2005.
- 948 [102] A C Fowler. A theory of glacier surges. *Journal of Geophysical Research*, 92(B9):9111–9120, 1987.
949 doi: 10.1029/JB092iB09p09111.

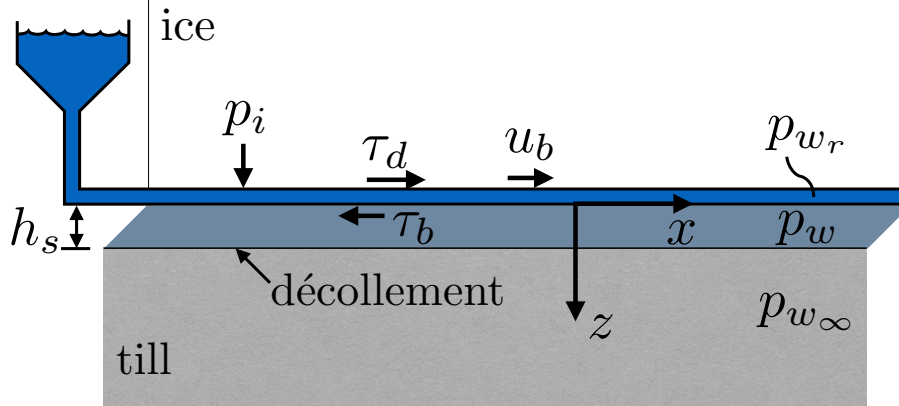


Figure 1: Model schematic showing a zoomed in view of the base of the idealized glacier with important parameters labeled.

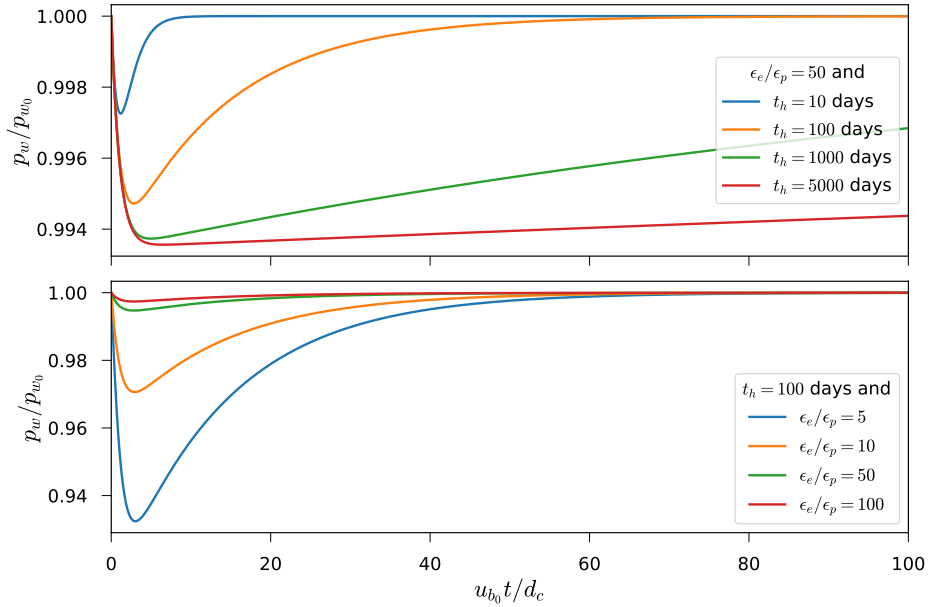


Figure 2: Evolution of pore water pressure in the deforming till layer (§33.1) following a step increase in basal slip rate, $u_b = 10u_{b_0}$ for $t \geq 0$, from an initial steady state ($\theta_0 = d_c/u_{b_0}$). The upper panel shows the influence of the hydraulic diffusion timescale of till on the evolution of pore water pressure for a fixed ϵ_e/ϵ_p ratio while the lower panel illustrates the influence of the ratio of the elastic to the plastic compressibility coefficients for a fixed diffusion timescale. Water pressures in the subglacial hydrological system (p_{w_r}) and underlying stagnant till layer (p_{w_∞}) are defined as $p_{w_r} = p_{w_\infty} = 0.9p_i$ and held constant in time. Other relevant parameters values are: $d_c = 0.1$, $\mu_n = 0.5$, $u_{b_0} = 10$ m/yr, $\phi_0 = 0.1$, and $p_{w_0} = p_{w_r} = p_{w_\infty}$.

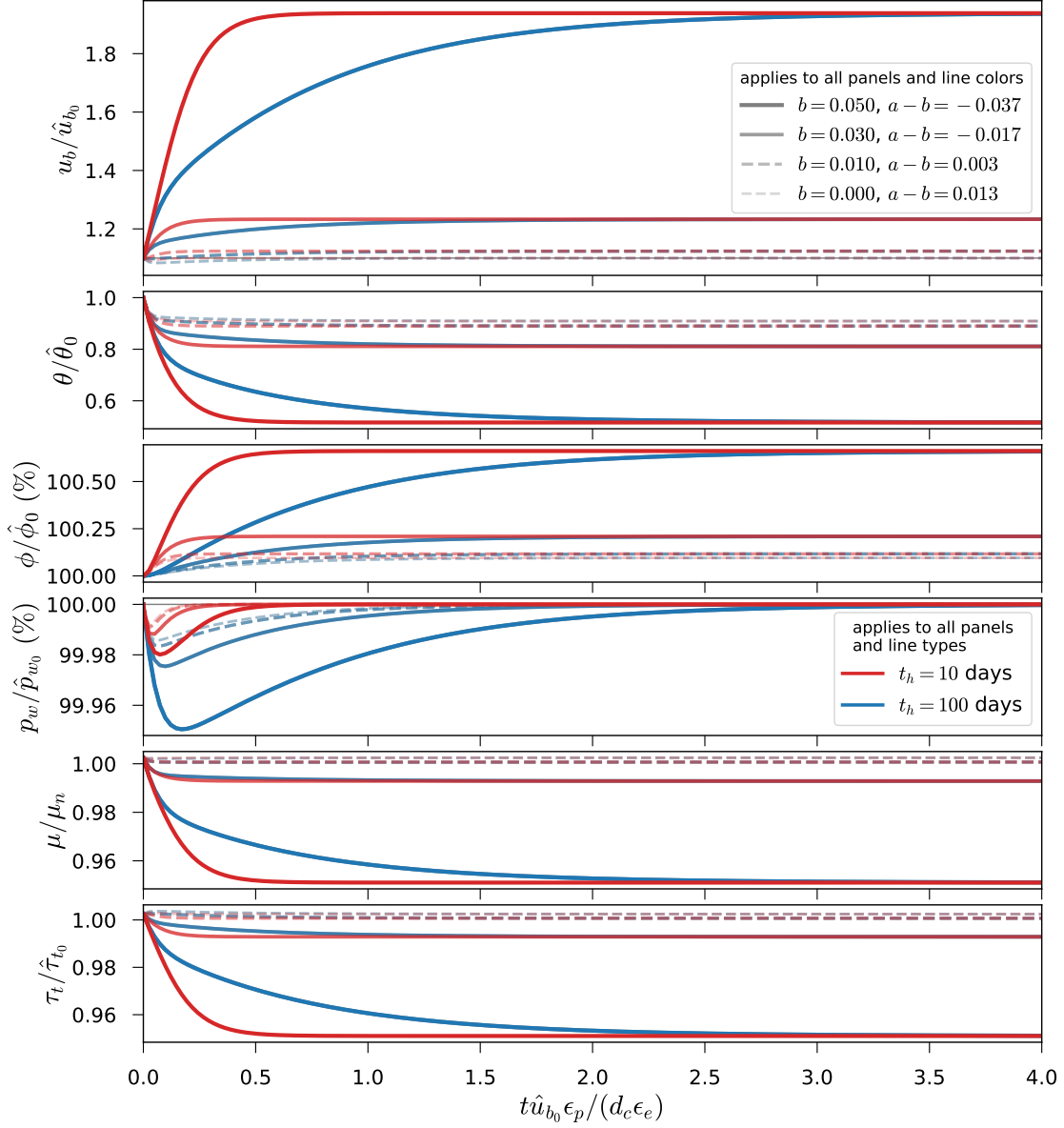


Figure 3: For fixed ice thickness §33.2: evolution of (from top to bottom) basal slip rate (u_b), state (θ), porosity (ϕ), pore water pressure in the deforming till layer (p_w), internal friction coefficient for till (μ), and till shear strength (τ_t) following a perturbation in basal slip rate from steady state. The perturbation in basal slip is $u_b = 1.1\hat{u}_b$ at $t = 0$, a value indicated by the thin solid gray line in the upper panel. We consider a range of evolution effects (b values, indicated by line widths and intensities in all panels) and two hydraulic diffusion timescales: $t_h = 10$ days (red lines in all panels) and $t_h = 100$ days (blue lines in all panels). In all panels, solid lines indicate rate-weakening ($a < b$) and dashed lines indicate rate-strengthening ($a > b$). Prescribed values are $\hat{u}_b = 10$ m/yr, $\hat{p}_w/p_i = 0.92$, $\hat{\phi}_0 = 0.1$, $d_c = 0.1$ m, $\epsilon_p = 10^{-3}$, $\epsilon_e = 50\epsilon_p$, $n = 3$, $\alpha = 0.05$, $a = 0.013$, and $\mu_n = 0.5$. Note that $d_c/\hat{u}_b = 0.01$ yr, making the total time on the horizontal axis 1 year. Here, we are interested in the response of the till only, so we hold glacier geometry constant.

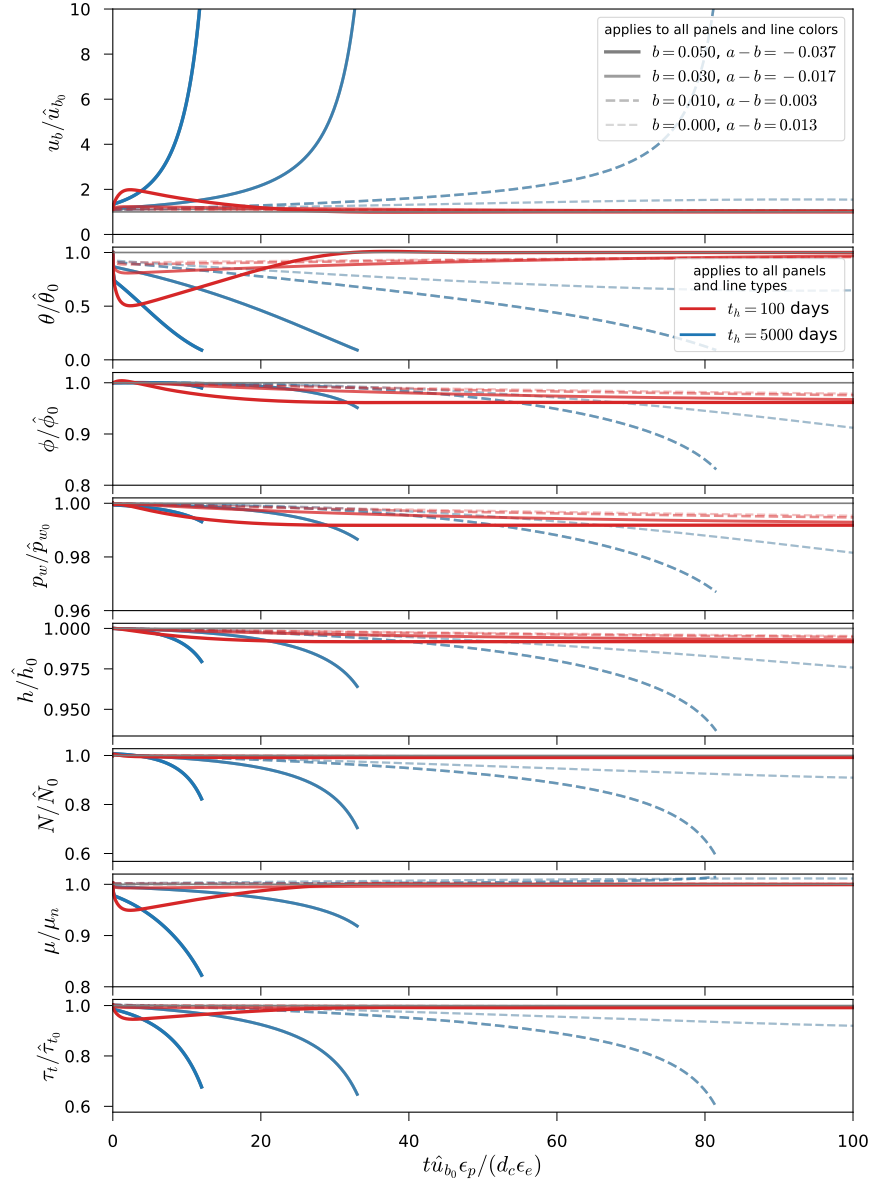


Figure 4: For variable ice thickness (§33.3): evolution of (from top to bottom) basal slip rate (u_b), state (θ), porosity (ϕ), pore water pressure in the deforming till layer (p_w), ice thickness (h), effective pressure (N), internal friction coefficient for till (μ), and till shear strength (τ_t) following a perturbation in basal slip rate from steady state. All factors are normalized by their respective initial steady state values. Velocity perturbation and other parameters are the same as for Fig. 3. Line thickness and continuity indicate different values of the evolution term b , as indicated in the legend in the upper panel, while line colors indicate values of the hydraulic diffusivity timescale for till (t_h), as shown in the legend in the third panel. Dashed lines indicate that the internal friction coefficient is rate-strengthening (*i.e.*, $(a - b) > 0$). Truncated lines occur when the integration is stopped; we chose $u_b/\hat{u}_{b0} = 10$, which we define as indicating a surge, as the stopping condition. Over a long enough timescale, the line representing $b = 0$ and $t_h = 5000$ days eventually surges.

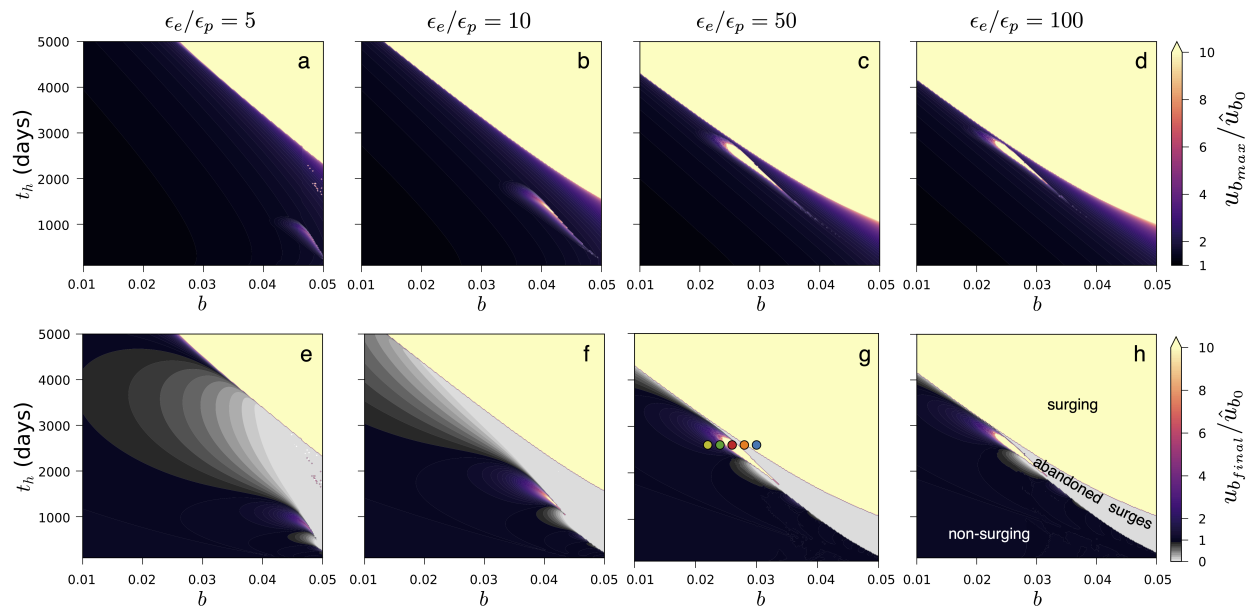


Figure 5: Parameter space covering the three principal parameters influencing incipient surge motion: the evolution effect b (x-axes of all panels), hydraulic diffusion timescale t_h (y-axes of all panels), and relative till compressibility ϵ_e/ϵ_p (columns). The top row (a–d) indicates the maximum basal slip rate ($u_{b,max}/\hat{u}_{b0}$) achieved by the modeled glacier following a perturbation identical to that in Fig. 4, while the bottom row (e–h) shows the final basal slip rate ($u_{b,final}/\hat{u}_{b0}$). Colored dots in (g) show the line colors and parameters for model outputs shown in Fig. 6. All other parameters are the same as in Fig. 4.

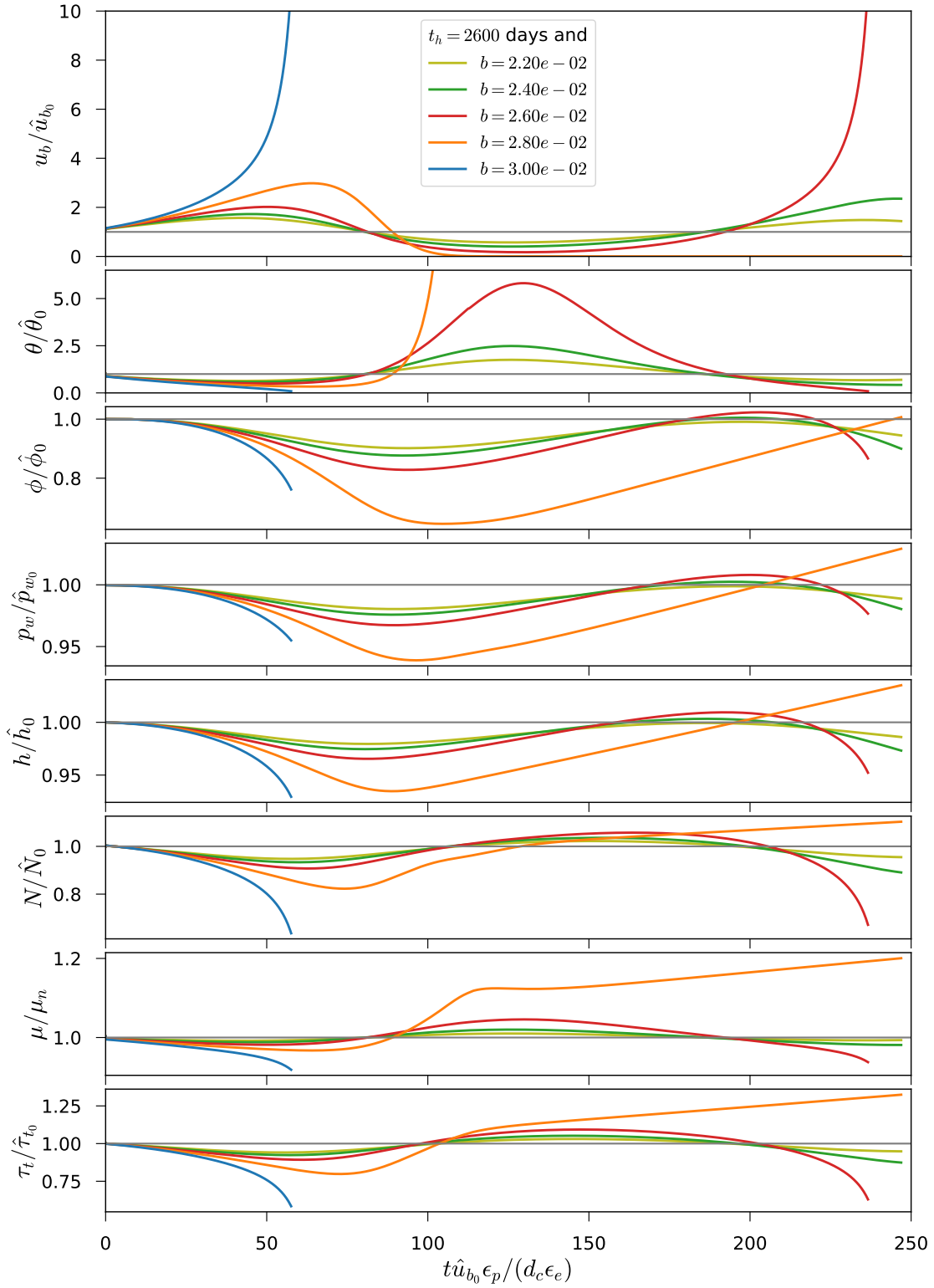


Figure 6: Similar to Fig. 4 except models are run using parameter values indicated in Fig. 5g. Line colors correspond to dot colors in Fig. 5g.

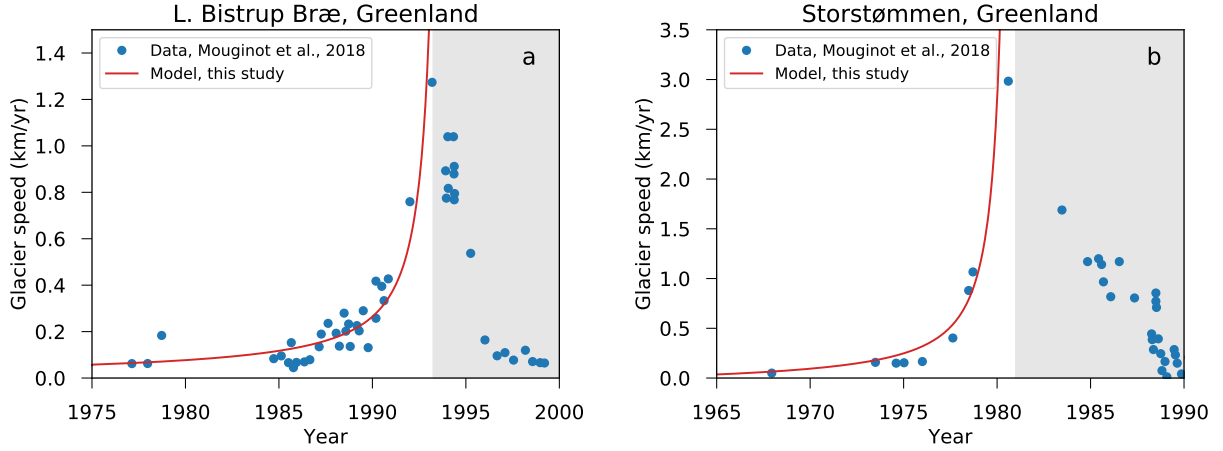


Figure 7: Comparison between our model and observed glacier surface velocities from two surges, (a) L. Bistrup Bræ and (b) Storstømmen, northeast Greenland [98]. Model parameters are the same as in Fig. 3 and 4, and with $b = 0.03$, $t_h = 3000$ days, and initial velocity set according to the data. The grayed regions indicate the slowdown phase of the surge, which our model does not attempt to represent.

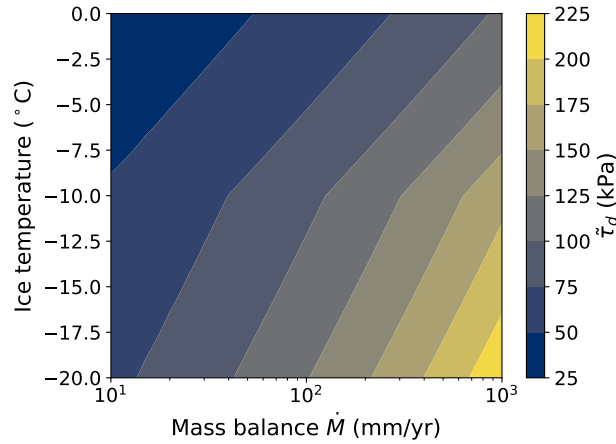


Figure 8: Potential drag at the bed $\tilde{\tau}_d$ (Eq. 36) as a function of surface mass balance (\dot{M}) and ice temperature. The rate factor is taken to depend on ice temperature T according to the Arrhenius relation $A = A_* \exp \{-Q_c (T^{-1} - T_*^{-1}) / R\}$, where $T_* = -10$ $^{\circ}\text{C}$, $A_* = 3.5 \times 10^{-25}$ $\text{Pa}^{-3} \text{s}^{-1}$, Q_c is the activation energy that increases from 60 kJ/mol for $T \leq T_*$ to 115 kJ/mol for $T_* < T \leq 0$ $^{\circ}\text{C}$, and $R = 8.314$ J/(K·mol) is the ideal gas constant [90].